New splicing variants of mitochondrial Rho GTPase-1 (Miro1) transport peroxisomes

Kanji Okumoto,[1,2] Tatsuaki Ono,[2] Ryusuke Toyama,[1] Ayako Shimomura,[1] Aiko Nagata,[2] and Yukio Fujiki[3]

[1]Department of Biology, Faculty of Sciences, [2]Graduate School of Systems Life Sciences, and [3]Division of Organelle Homeostasis, Medical Institute of Bioregulation, Kyushu University, Fukuoka, Japan

Microtubule-dependent long-distance movement of peroxisomes occurs in mammalian cells. However, its molecular mechanisms remain undefined. In this study, we identified three distinct splicing variants of human mitochondrial Rho GTPase-1 (Miro1), each containing amino acid sequence insertions 1 (named Miro1-var2), 2 (Miro1-var3), and both 1 and 2 (Miro1-var4), respectively, at upstream of the transmembrane domain. Miro1-var4 and Miro1-var2 are localized to peroxisomes in a manner dependent on the insertion 1 that is recognized by the cytosolic receptor Pex19p. Exogenous expression of Miro1-var4 induces accumulation of peroxisomes at the cell periphery and augments long-range movement of peroxisomes along microtubules. Depletion of all Miro1 variants by knocking down *MIRO1* suppresses the long-distance movement of peroxisomes. Such abrogated movement is restored by reexpression of peroxisomal Miro1 variants. Collectively, our findings identify for the first time peroxisome-localized Miro1 variants as adapter proteins that link peroxisomes to the microtubule-dependent transport complexes including TRAK2 in the intracellular translocation of peroxisomes in mammalian cells.

Introduction

A single membrane-bound organelle, peroxisome, catalyzes essential catabolic and anabolic reactions such as detoxification of hydrogen peroxide, β-oxidation of very long chain fatty acids, and the synthesis of ether phospholipids (Wanders, 2014). Recent advances including identification of several *PEX* genes have revealed that peroxisomal homeostasis involving regulation of the number, morphology, and metabolic functions of peroxisomes is maintained by coordinating biogenesis, proliferation, division, and degradation of peroxisomes (Fujiki et al., 2014). In addition, intracellular movement of peroxisomes is observed in many organisms and is thought to contribute to inheritance, spatial distribution, and functions of peroxisomes (Knoblach and Rachubinski, 2015; Neuhaus et al., 2016).

Intracellular organelles are transported by molecular motors along the cytoskeletons of microtubular networks or actin filaments, which requires a highly specific organelle–motor relationship via direct or adapter protein–mediated interactions (Hirokawa et al., 2009; Kardon and Vale, 2009). In *Saccharomyces cerevisiae*, a peroxisomal membrane protein (PMP), Inp2, interacts with the type V myosin motor Myo2 to transport peroxisomes along actin cables to the bud (Fagarasanu et al., 2006, 2009). In mammalian cells, peroxisomes show two types of motility: one for relatively slow oscillation observed in the majority and the other for fast directional long-distance movement in a microtubule-dependent manner as for the transport of other organelles in mammals (Rapp et al., 1996; Wiemer et al., 1997; Schrader et al., 2000; Bharti et al., 2011; Fan et al., 2014). The long-range movement of peroxisomes is shown to require a PMP, Pex14p, that directly binds to tubulin (Bharti et al., 2011). Furthermore, involvement of the microtubule-dependent motors KifC3 (Dietrich et al., 2013) and dynein (Schrader et al., 2000) in peroxisomal movement are suggested in mammalian cells. These observations implicate a linkage between peroxisomes and microtubule-associated molecular motors. However, molecular mechanisms underlying intracellular transport of peroxisomes in mammals remain largely undefined mainly because of a lack of peroxisomal adapter protein or proteins linking peroxisomes to an unknown specific motor complex.

The molecular basis of mitochondrial transport is better elucidated. Mitochondrial Rho GTPase (Miro) proteins localized to mitochondrial outer membrane (MOM) belong to a family of tail-anchored (TA) membrane proteins (Saxton and Hollenbeck, 2012; Birsa et al., 2013; Schwarz, 2013; Sheng, 2014). Two Miro family members, Miro1 and Miro2, are identified in mammalian cells (Fransson et al., 2003). Recent studies revealed that mammalian Miro proteins interact with the adapter proteins TRAK1 and TRAK2, which recruit microtubule-associated molecular motors in the transport of mitochondria (Glater et al., 2006; Wang and Schwarz, 2009). Miro1-mediated mitochondrial transport is regulated by cytosolic calcium ion concentration (Saotome et al., 2008; MacAskill et al., 2009b; Wang and Schwarz, 2009; Chen and Sheng, 2013) and its GTPase activity (MacAskill et al., 2009a; Babic et al., 2015).

Correspondence to Yukio Fujiki: yfujiki@kyudai.jp

The Rockefeller University Press
J. Cell Biol. Vol. 217 No. 2 619–633
https://doi.org/10.1083/jcb.201708122

Targeting of PMPs to peroxisomes requires the peroxisomal membrane-targeting signal (mPTS) and its cytosolic receptor Pex19p (Jones et al., 2004; Matsuzono et al., 2006). Like most PMPs (Jones et al., 2004; Halbach et al., 2005; Matsuzono et al., 2006; Matsuzaki and Fujiki, 2008; Chen et al., 2014; Liu et al., 2016), a mammalian peroxisomal TA protein, Pex26p, is posttranslationally targeted from the cytosol to peroxisomes via the Pex19p- and Pex3p-dependent class I pathway (Yagita et al., 2013). The C-terminal region of Pex26p, containing a transmembrane domain (TMD) with relatively low hydrophobicity and a following short cluster of basic amino acids, allows specific recognition by Pex19p and escape from capture by TRC40 (Yagita et al., 2013), the import receptor of ER-destined TA proteins in the guided entry of the TA protein pathway (Hegde and Keenan, 2011). TA proteins localized to MOM appear to be transported by the unassisted pathway (Brambillasca et al., 2005; Setoguchi et al., 2006; Kemper et al., 2008). Moreover, a part of TA proteins targets multiple organelles, conferring more complexity in TA protein import (Borgese and Fasana, 2011; Rao et al., 2016). The mechanisms underlying such selective localization of TA proteins are not fully elucidated. Most recently, analysis of subcellular localization for human TA proteins suggested a subset of TA proteins including Miro proteins dually localized to peroxisomes and mitochondria (Costello et al., 2017a).

In this study, we identified three splicing variants of Miro1 termed Miro1-var2, Miro1-var3, and Miro1-var4 in human cells. Miro1-var2 and Miro1-var4 were partially and mostly localized to peroxisomes, respectively, and both are involved in microtubule-dependent long-range movement of peroxisomes.

Results

Identification of three distinct splicing variants of Miro1

In RT-PCR for cloning of human *Miro* cDNAs, we identified three distinct splicing variants of Miro1, named Miro1-var2, -var3, and -var4, in addition to authentic well-characterized Miro1 (hereafter termed Miro1-var1) and Miro2, C-TA–type MOM proteins (Fig. 1 A). Compared with 618-aa Miro1-var1, Miro1-var2 and Miro1-var3 contained 32 and 41 aa insertions, termed insertions 1 and 2, respectively (Fig. 1 A, pink and orange), and Miro1-var4 contained both insertions. These insertions were located between the second GTPase domain and the TMD of Miro1-var1 (Fig. 1 A). Genomic information of the DNA database indicated that insertions 1 and 2 of Miro1 variants were encoded by the alternatively spliced putative 19th and 20th exons of human *Miro1* gene, respectively (Figs. 1 A and S1 A). Similar genome structure and splicing variants of Miro1 were also found in mice (Fig. S1 B). Semiquantitative RT-PCR to amplify the alternative splicing region of *Miro1* variants (Fig. 1 A) showed that mRNA of each splicing variant of *Miro1* was expressed at varying levels in HeLa cells (Fig. 1 B). Compared with predominantly expressed *Miro1-var1* and *Miro1-var2*, *Miro1-var3* and *Miro1-var4* were expressed at ∼10% and a lesser levels, respectively, of *Miro1-var1* and *Miro1-var2* (Fig. 1 B). A similar expression profile of *Miro1* variant mRNAs was found in HEK cells (Fig. S1 C) and various mouse tissues except for testis, where Miro1-var4 mRNA was highly expressed (unpublished data). A search for genome DNA database showed that both insertions 1 and 2 are conserved in *Miro1* genes in mammals; only the insertion 2 is found in other vertebrates such as *Gallus gallus* (chicken) and *Xenopus tropicalis* (frog; Fig. S1 D). These results suggested that the splicing variants of *Miro1* with the unique insertions are specifically expressed in mammals.

Miro1-var2 and Miro1-var4 localize to peroxisomes

We investigated intracellular localization of the splicing variants of Miro1. N-terminally tandem HA–tagged splicing variants of Miro1 (HA_2-Miro1 variants) were expressed in HeLa cells at a lower expression levels by transfecting 1/10 of the amount of plasmids used for typical transfection assays to avoid mislocalization by incorrect targeting. HA_2–Miro1-var3 was entirely coincided with a MOM protein Tom20 (Fig. 1 C, i–k; and Fig. 1 D), indicating that its mitochondrial localization is like an authentic Miro1 variant, HA_2-Miro1-var1 (Fig. 1 C, a–d; and Fig. 1 D; Fransson et al., 2003). Notably, in ∼75% of the cells expressing the longest HA_2–Miro1-var4, Miro1-var4 was localized to Pex14p-positive particle structures, peroxisomes, whereas in the remaining 25% of cells, it was discernible in mitochondria and peroxisomes (Fig. 1 C, m–p; and Fig. 1 D). HA_2–Miro1-var4 localizing to peroxisomes showed no significant effect on mitochondrial morphology (Fig. 1 C, o). Localization of HA_2–Miro1-var2 was classified into two types: ∼60% was found in both mitochondria and peroxisomes, and the rest was exclusively in mitochondria (Fig. 1 C, e–h; and Fig. 1 D). Similar peroxisomal localization patterns were observed in the FLAG-EGFP–tagged C-terminal regions of Miro1 (termed MVC) encompassing the TMD and the respective insertions of Miro1-var4 and Miro1-var2, named FL-EGFP-MV4C and MV2C, respectively (Fig. S2, A–C). FL-EGFP-MV3C was detected only in mitochondria, as was FL-EGFP-MV1C (Fig. S2, A–C), consistent with an earlier study (Fransson et al., 2006). These results strongly suggest that Miro1-var4 and Miro1-var2 are mainly and partially localized to peroxisomes, respectively, in a manner dependent on the insertion 1.

Miro1 variants localize to peroxisomes as a TA membrane protein

To further investigate peroxisomal localization of Miro1 variants, we raised a rabbit polyclonal antibody against a 32-aa peptide corresponding with the insertion 1, named anti–Miro1-ins1 antibody. In immunoblot analysis, this antibody specifically recognized human Miro1-var2 and Miro1-var4, which were expressed in CHO cells (Fig. 2 A, top, lanes 5 and 6). The antibody was not cross-reactive to the other Miro1 variants and Miro2 (Fig. 2 A, top, lanes 2–4). We used another type of anti-Miro1 antibody, termed the anti-Miro1/2 antibody, reactive to all of the four Miro1 variants and Miro2 (Fig. 2 A, bottom, lanes 1–6). In subcellular fractionations of the postnuclear supernatant (PNS) fraction of HEK cells, several contiguous bands were detected by anti-Miro1/2 antibodies (Fig. 2 B), which were suspected to be three Miro1 variants other than Miro1-var4, and Miro2 was detected by mRNA expression level of Miro1 variants (Fig. S1 C) and their mobility (Fig. 2 A, bottom). These bands showed a distribution pattern similar to that of the MOM protein Tom20, hence suggesting that Miro1-var1, Miro1-var2, Miro1-var3, and Miro2 are located on mitochondria (Fig. 2 B).

Notably, a portion of proteins recognized by anti–Miro1-ins1 antibody was found in heavier fractions up to fraction 2, where PMP Pex3p was enriched (Fig. 2 B), whereas the proteins were mostly present in mitochondrial fractions. The band

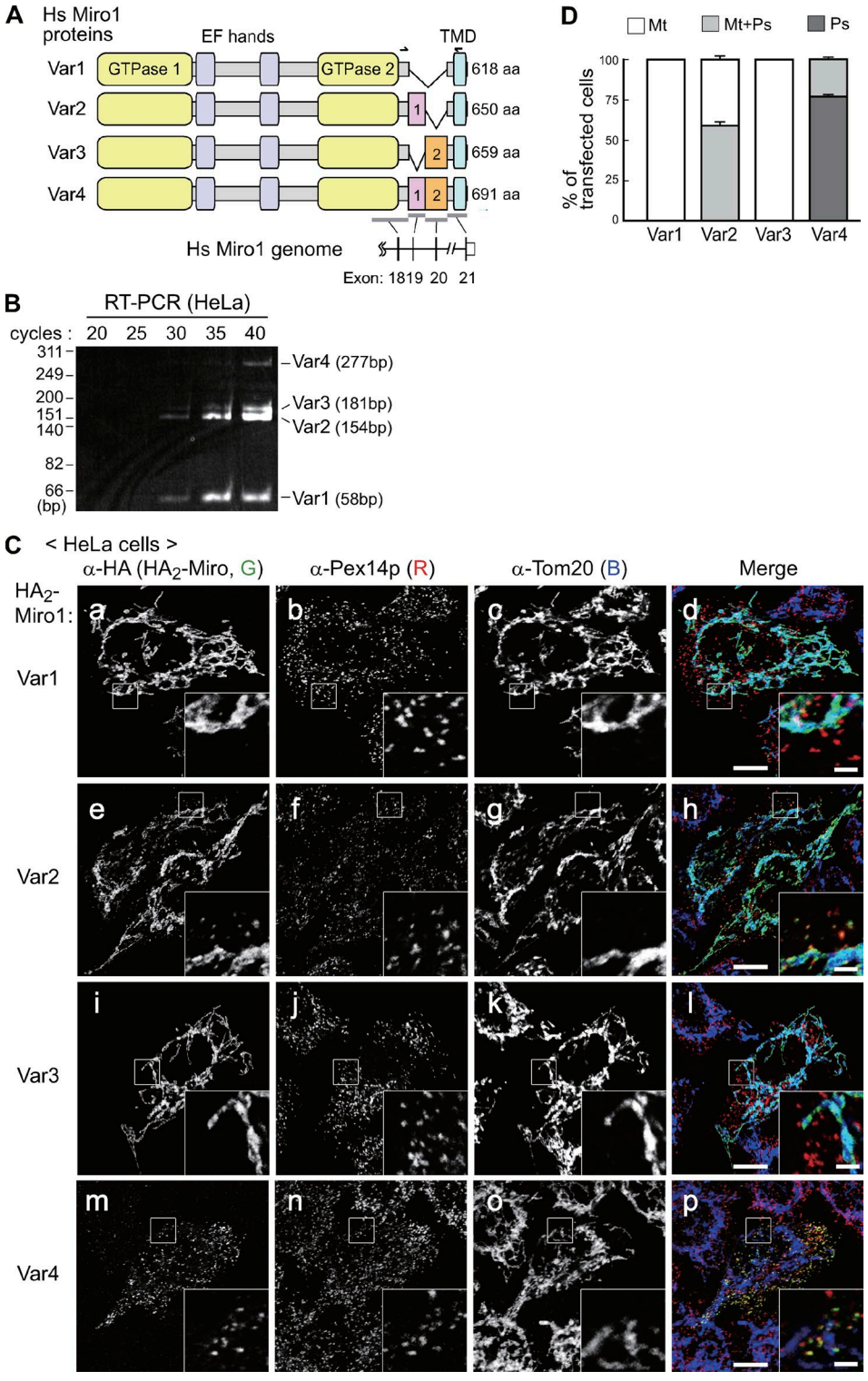

Figure 1. **Distinct intracellular localization of splicing variants of Miro1. (A)** Domain structure of human authentic Miro1 and three splicing variants of Miro1. EF hands, calcium-binding EF hand domains. Partial genome structure of the human *MIRO1* gene encoding the C-terminal region of Miro1 variants is shown at the bottom. Pink and orange boxes indicate the insertions 1 and 2 generated by alternative splicing of exons 19 and 20, respectively. Primers for RT-PCR are shown by half-arrowheads at the top. **(B)** Expression of mRNA of *MIRO1* splicing variants in HeLa cells. Human *MIRO1* encoding the C-terminal variable region of Miro1 was amplified by semiquantitative RT-PCR with RNA from HeLa cells and a pair of primers shown in A. Size markers are shown on the left. **(C)** Intracellular localization of splicing variants of Miro1. HA_2-Miro1 variants were assessed by transient expression in HeLa cells for 24 h and immunostaining with antibodies to HA (a, e, i, and m; green), Pex14p (b, f, j, and n; red), and Tom20 (c, g, k, and o; blue). Merged images are shown (d, h, l, and p), and the boxed areas were magnified 3.5-fold in insets. Representative images are shown. Bars: (main images) 10 μm; (insets) 2 μm. **(D)** Data in C were quantified for localization of respective Miro1 variants to mitochondria (Mt; white), peroxisomes (Ps; dark gray), and both (Mt+Ps; light gray). Data are shown as means ± SD. Transfected cells ($n \geq 100$) for each condition were counted in three independent experiments.

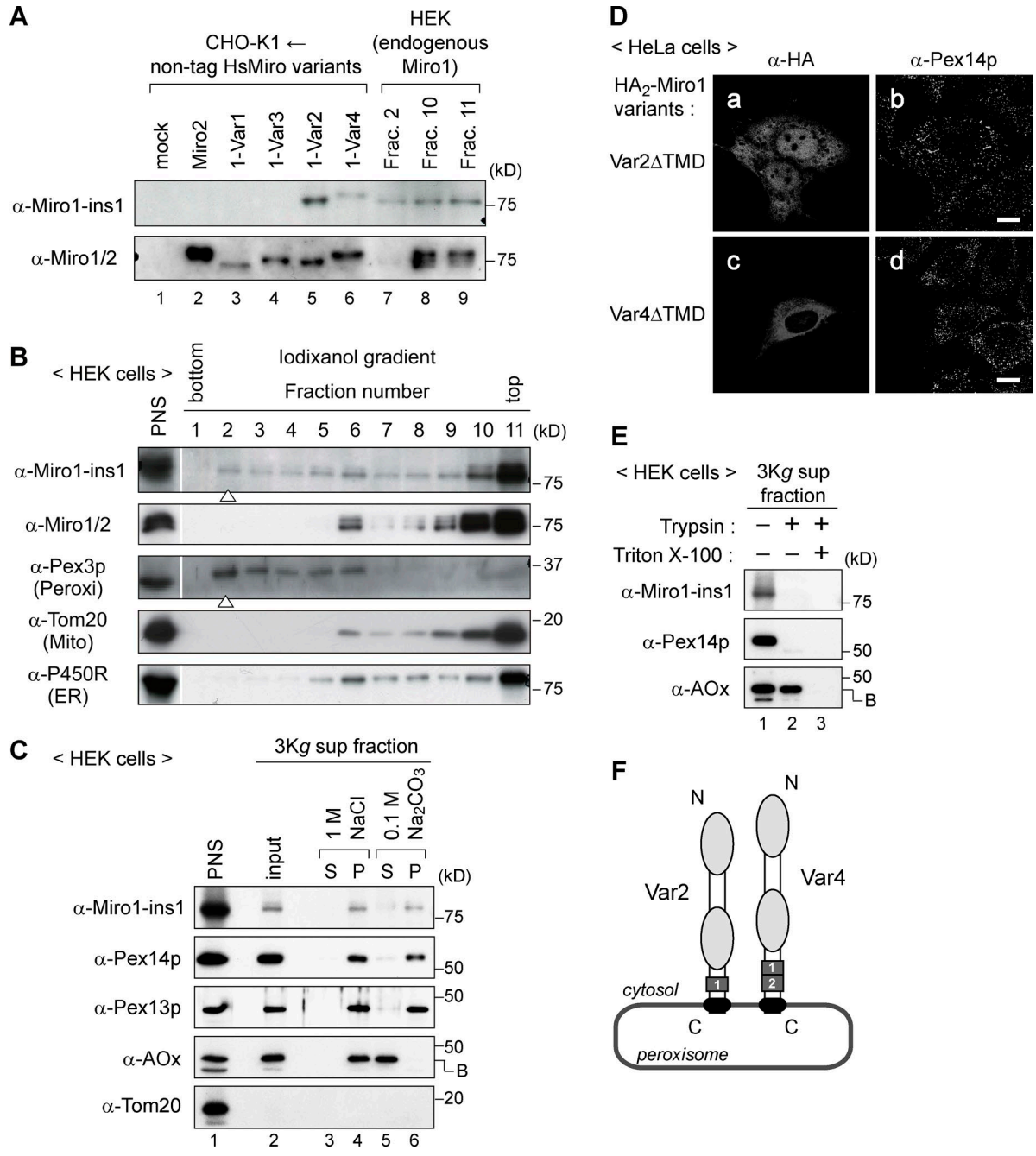

Figure 2. **Peroxisomal localization of endogenous Miro1 variants. (A)** To verify two types antibodies raised to Miro1 and migration of Miro variants in SDS-PAGE, lysates of CHO-K1 cells transfected with nontagged *Miro2* (lane 2), *Miro1* variants (lanes 3–6), and a mock plasmid (lane 1) were analyzed by immunoblotting. Note that anti–Miro1-ins1 antibody specifically recognizes Miro1-var2 and Miro1-var4 (lanes 5 and 6), whereas anti-Miro1/2 antibody detects all of the Miro1 variants and Miro2 (lanes 2–6). Fraction 2 (lane 7) and half and one-eighth aliquots of fractions 10 and 11, respectively (lanes 8 and 9), from subcellular fractions of HEK cells in B were similarly analyzed. **(B)** Subcellular fractionation of HEK cells. PNS fraction of HEK cells was fractionated in iodixanol density gradient as described in the Subcellular fractionation section of Materials and methods. Equal-volume aliquots of the collected fractions were analyzed by SDS-PAGE and immunoblotting with antibodies indicated on the left. Cytochrome P450 reductase (P450R), Tom20, and Pex3p are markers for ER, mitochondria (Mito), and peroxisomes (Peroxi), respectively. Arrowheads indicate fractions of highly purified peroxisomes. White lines indicate intervening lanes have been spliced out. **(C)** Peroxisomal Miro1-var2 is an integral membrane protein. PNS fraction of HEK cells was centrifuged at 3,000 *g*, and the supernatant (S; 3K*g* sup) fraction was divided into three aliquots. One aliquot was directly lysed in Laemmli sample buffer (input). The other two were separately treated with 1 M NaCl and 0.1 M Na_2CO_3, respectively, and separated into supernatant and pellet (P) fractions. Equal aliquots of respective 3K*g* sup fractions and a PNS fraction were analyzed by SDS-PAGE and immunoblotting with antibodies specific for the insertion 1 of Miro1, Tom20, the PMPs Pex14p and Pex13p, and acyl-CoA oxidase (AOx), a peroxisomal matrix enzyme. Only the B chain of AOx that is produced by intraperoxisomal processing of full-length AOx is shown. **(D)** TMD of Miro1-var2 and Miro1-var4 is required for their localization to peroxisomes. HeLa cells transiently transfected with *HA_2–Miro1-var2ΔTMD* (a and b) and *HA_2–Miro1-var4ΔTMD* (c and d) were immunostained with antibodies to HA and Pex14p as in Fig. 1 C. Bars, 10 µm. **(E)** Membrane topology of endogenous Miro1-var2 in peroxisomes. The 3K*g* sup fraction of HEK cells was incubated for 30 min on ice in the absence (lane 1) or presence of 100 µg/ml trypsin alone (lane 2) and both trypsin and 0.1% Triton X-100 (lane 3). Equal aliquots were analyzed by SDS-PAGE and immunoblotting with indicated antibodies, including the anti-Pex14p antibody specific for the cytosolically faced C-terminal part of Pex14p. **(F)** Schematic diagram of the topology of Miro1-var2 and Miro1-var4 in peroxisomes. Dark gray boxes, insertions 1 and 2; black and light gray ellipses, a TMD and two GTPase domains, respectively.

detected by anti–Miro1-ins1 antibody in fraction 2 as well as fractions 10 and 11 showed the mobility identical to Miro1-var2 (Fig. 2 A, lanes 5 and 7–9). Collectively, these results indicated that at least endogenous Miro1-var2 is partially localized in peroxisomes in HEK cells, consistent with immunostaining of HA_2–Miro1-var2 (Fig. 1 C, e–h). Although Miro1-var4 was possibly present in peroxisomes, endogenous Miro1-var4 was below the detectable level even in peroxisome-enriched fractions in HEK cells, presumably because of much lower expression of the mRNA (Fig. S1 C) and inefficient recognition by anti–Miro1-ins1 antibody (Fig. 2 A, compare lanes 5 and 6).

Next, membrane topology of peroxisome-localized Miro1 variants was assessed. In a post-heavy mitochondria fraction enriched in peroxisomes and almost devoid of mitochondria, endogenous Miro1-var2 was resistant to high-salt washing and alkaline extraction, indicative of an integral membrane protein as for typical PMPs such as Pex14p and Pex13p (Fig. 2 C). Consistent with this result, truncated mutants of HA_2–Miro1-var4 and HA_2–Miro1-var2 lacking their C-terminal TMD were diffused in the cytosol (Fig. 2 D), hence indicating that TMD is essential for their peroxisomal localization, similar to mitochondrial anchoring of Miro1-var1 (Fransson et al., 2006). The region including insertion 1 of Miro1-var2 was sensitive to trypsin digestion in the absence of detergent Triton X-100, showing that the N-terminal region was faced to cytosol exactly as the C-terminal region of Pex14p was (Fig. 2 E; Shimizu et al., 1999). Furthermore, immunostaining of HeLa cells semipermeabilized with digitonin demonstrated that the N-terminal part of HA_2–Miro1-var4 and HA_2–Miro1-var2 were exposed to the cytosol (Fig. S2 D). Collectively, we concluded that Miro1-var2 and presumably Miro1-var4 are localized to peroxisomes as a TA membrane protein with the same topology as mitochondrial Miro1-var1 (Fig. 2 F). Miro1-var4 was mainly used for further studies.

Peroxisomal localization of Miro1-var4 and Miro1-var2 is dependent on its insertion 1– and Pex19p-mediated PMP import pathway

Pex19p recognizes peroxisomal TA proteins such as Pex26p via mPTS-containing C-terminal regions (Halbach et al., 2006; Yagita et al., 2013). To investigate whether Pex19p is involved in peroxisomal import of Miro1-var4 and Miro1-var2, Miro1 variants were examined for binding to Pex19p. In the cell-free immunoprecipitation assay using proteins synthesized in a rabbit reticulocyte lysate (RRL) translation system, the C-terminal regions of Miro1-var4 and Miro1-var2 but not Miro1-var1 and Miro1-var3 interacted with HA_2-Pex19p to a lesser extent than that of Pex26p (Fig. 3 A). This was well correlated with the insertion 1–dependent peroxisomal localization of Miro1-var4 and Miro1-var2 (Figs. 1 B and S2 B), suggesting a potential Pex19p binding site in the insertion 1. Indeed, we found amino acid sequences at the C-terminal parts of insertion 1 and adjacent linker regions in Miro1-var4 and Miro1-var2 that were similar to typical Pex19p-binding sites, including the core 9-aa sequences each identified in Pex13p and Pex11p of *S. cerevisiae* and human adrenoleukodystrophy protein (Fig. 3 B; Rottensteiner et al., 2004; Halbach et al., 2005). Therefore, leucine 608, one of the highly conserved residues in the insertion 1 was substituted to proline in FL-EGFP-MVC variants of Miro1-var4 and Miro1-var2, corresponding with the mutations L207P in *Sc*Pex13p and L35P in *Sc*Pex11p, both defective in interaction with Pex19p (Rottensteiner et al., 2004). L608P mutation abrogated the interaction of Miro1-var4 and Miro1-var2 with Pex19p in vitro (Fig. 3 C), leading to mislocalization of Miro1-var4 and Miro1-var2 to mitochondria (Fig. 3 D). Furthermore, overexpressed WT FL-EGFP-MV4C and FL-EGFP-MV2C, but not those with L608P mutation, were partly stabilized in the cytosol upon coexpression of Pex19p (Fig. S3 A) as shown in several PMPs including Pex26p (Sacksteder et al., 2000; Jones et al., 2004; Yagita et al., 2013; Liu et al., 2016). L608P mutation likewise interfered with peroxisomal localization of full-length Miro1-var4 (Fig. S3 C, a–d) and Miro1-var2 (e–h). These results further supported that C-terminal region of the insertion 1 is a primary Pex19p binding site. Basic amino acid residues in the hydrophilic luminal region were shown to be also important for peroxisomal targeting of TA proteins (Yagita et al., 2013). Replacement of the two basic amino acids located within putative luminal regions of Miro1-var4 and Miro1-var2 by serine residues (named KR2S; Fig. 3 B) markedly lowered the efficiency of their peroxisomal localization, resulting in mislocalization predominantly to mitochondria (Fig. S3 B). These results show that both insertion 1 and the basic charge in luminal region are essential for the efficient localization of Miro1-var4 and Miro1-var2 to peroxisomes. Tandem positioning of the insertions 1 and 2 potentially elevated the targeting efficiency of Miro1-var4 to peroxisomes.

Next, we performed peroxisomal import of Miro1-var4 and Miro1-var2 by an in vitro PMP import assay system using semiintact cells (Matsuzaki and Fujiki, 2008; Yagita et al., 2013; Liu et al., 2016). When cytosolic fractions prepared from the cells coexpressing HA_2–Miro1-var4 or HA_2–Miro1-var2 with FLAG-Pex19p were incubated with semiintact HeLa cells, both HA_2-Miro1 variants were detected exclusively in Pex14p-positive particles, peroxisomes (Fig. 3 E, a–d), with lower efficiency than HA_2-Pex26p (e and f). Miro1-var4 and Miro1-var2 targeted to peroxisomes were mostly integrated into the peroxisomal membrane as assessed by resistance to the alkaline extraction (Fig. 3 F). Collectively, these results strongly suggest that Pex19p interacts with Miro1-var4 and Miro1-var2 via their insertion 1 and delivers them to peroxisomes.

Miro1-var4 promotes microtubule-dependent accumulation of peroxisomes at cell periphery

Miro1-var1 mediates intracellular transport of mitochondria as a mitochondrial receptor by forming a microtubule-dependent transport complex in which its GTPase activity is important (MacAskill et al., 2009a; Babic et al., 2015). By analogy to mitochondrial Miro1-var1, we investigated whether peroxisomal Miro1 variants are involved in intracellular transport of peroxisomes. Notably, expression of HA_2–Miro1-var4 in HeLa cells often induced accumulation of peroxisomes, but not mitochondria, at the cell periphery (Fig. 4 A, arrowheads). About 60% of the cells expressing WT Miro1-var4 showed such accumulation of peroxisomes at the cell periphery (Fig. 4 B, a–c; and Fig. 4 C). Two GTPase-1 mutants of Miro1-var1, a constitutively active P13V mimicking its GTP-bound form and a dominant-negative T18N defective in GTP binding, exhibit similar and much fewer activities, respectively, as compared with WT in mitochondrial transport (MacAskill et al., 2009a). An analysis using the corresponding GTPase-1 mutant of Miro1-var4, Miro1-var4–P13V, yielded clustered peroxisomes with efficiency similar to WT Miro1-var4, whereas Miro1-var4–T18N exhibited much fewer numbers of the accumulated peroxisomes

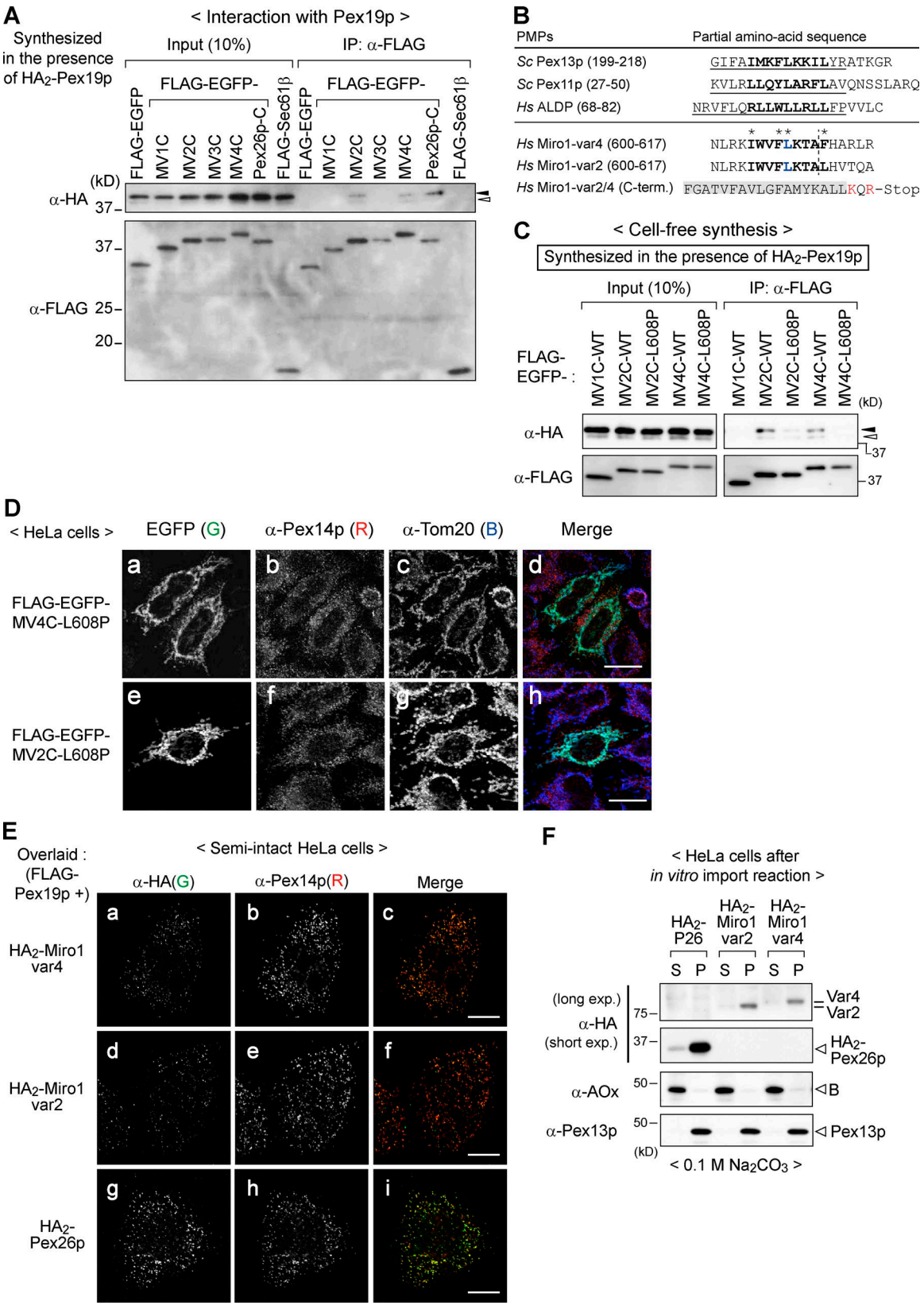

Figure 3. **Miro1-var2 and Miro1-var4 are translocated to peroxisomes in a manner dependent on their specific insertion 1 and the PMP receptor Pex19p. (A)** FLAG-EGFP–fused C-terminal regions of Miro1 variants (FL-EGFP-MVCs) indicated at the top were synthesized in RRL in the presence of RRL-synthesized HA_2-Pex19p and subjected to immunoprecipitation (IP) with anti-FLAG agarose beads. Immunoprecipitates and input (10%) were analyzed by immunoblotting using antibodies to HA and FLAG. Solid and open arrowheads indicate unmodified and farnesylated HA_2-Pex19p, respectively. **(B)** Partial amino acid sequences near the C terminus of insertion 1 of human Miro1-var2 and Miro1-var4 are aligned with those of known Pex19p binding sites such as those of *S. cerevisiae* Pex13p and Pex11p and human adrenoleukodystrophy protein (ALDP). Underlined and bold letters indicate experimentally identified

(Fig. 4 C). However, peroxisomal accumulation at the cell periphery was hardly observed in cells expressing WT Miro1-var1 and its mutants P13V and T18N (Fig. 4 C). Importantly, accumulation of peroxisomes induced by a lower-level expression of Miro1-var4 was completely abolished by treatment of nocodazole, a microtubule-depolymerizing agent (Fig. 4 B, d–f; and Fig. 4 C). These results suggest that Miro1-var4 is specifically involved in the peroxisomal transport toward plus ends of the microtubule network in a manner dependent on its GTPase activity and microtubules.

Peroxisomal Miro1 variants are involved in intracellular movement of peroxisomes

Given that Miro1-var1 regulates mitochondrial transport (Saxton and Hollenbeck, 2012; Birsa et al., 2013; Schwarz, 2013; Sheng, 2014) and Miro1-var4 is involved in intracellular transport of peroxisomes (Fig. 4), it is particularly of interest and importance to investigate peroxisomal movement in living cells. We used HeLa cells stably expressing peroxisome-targeted EGFP (EGFP fused with a tripeptide consisting of Ser-Lys-Leu at its C terminus; EGFP-SKL), named HeLa/EGFP-SKL, to acquire time-lapse images of peroxisomal motility (Fig. 5 A). In this experiment, the directional movement frequency (DMF) of peroxisomes was defined as a rate of a directional movement of peroxisomes that were >0.5 µm/s in velocity and >2 µm in distance in total peroxisomes for 5-min measurements. Under normal conditions, ∼10% of total peroxisomes moved fast and directionally in HeLa/EGFP-SKL cells (Fig. 5, A and B; and Video 1) and likewise in CV1 cells (Wiemer et al., 1997). Transient expression of mCherry-tagged WT Miro1-var4 increased DMF by 2.5-fold (Fig. 5 B and Video 2), whereas GTPase-inactive mCherry–Miro1-var4–T18N gave rise to a marked decrease of DMF, indicative of its dominant-negative effect (Fig. 5 B). Tagging of mCherry to Miro1 variants showed no effects on their localization, as assessed by immunostaining (Fig. S4 A). Nocodazole treatment almost completely abrogated DMF in normal cells (Fig. 5 C), suggesting that directional movement of peroxisomes was regulated in a manner dependent on microtubule and GTPase activity of Miro-var4. The peroxisome movement represented by DMF was consistent with the accumulation of peroxisomes at cell peripheries (Fig. 4).

In contrast, when all of the Miro1 variants were knocked down in HeLa/EGFP-SKL cells by *Miro1* siRNA treatment (Fig. 5 D), the DMF of peroxisomes was significantly reduced to a level similar to that in nocodazole-treated cells (Fig. 5, C and E; and Videos 3 and 4). To determine which Miro1 variants were responsible for the fast directional movement of peroxisomes, RNAi-resistant forms of mCherry-Miro1 variants, named rescue variants, were reintroduced into Miro1-depleted HeLa/EGFP-SKL cells. A rescue variant mCherry–Miro1-var4 restored the compromised peroxisomal movement and further enhanced the DMF value to ∼24% (Fig. 5 E and Video 5), a comparable level to that in normal cells expressing mCherry–Miro1-var4 (Fig. 5 B and Video 2). DMF was similarly rescued by mCherry–Miro1-var2 (Fig. 5 E and Video 6) but not mCherry–Miro1-var1 (Fig. 5 E). Collectively, these results suggest that Miro1-var2 and Miro1-var4, both localized to peroxisomes, play a pivotal role in intracellular transport of peroxisomes.

Pex14p, a main component in the peroxisomal protein translocation machinery, was shown to directly interact with microtubules, and the fast peroxisomal movement was not observed in *PEX14*-deficient cells (Bharti et al., 2011). Therefore, we verified Miro1 variant–dependent peroxisomal movement in fibroblasts derived from a *PEX14*-deficient patient with Zellweger syndrome (Shimozawa et al., 2004). In normal fibroblasts, HA_2–Miro1-var4 was colocalized with EGFP-Pex26p in Pex14p-positive peroxisomes and induced the accumulation of peroxisomes at cell peripheries (Fig. 5 F, a–d, arrowheads; and Fig. 5 G) as observed in HeLa cells (Fig. 4 A). In *PEX14*-deficient fibroblasts defective in matrix protein import, HA_2–Miro1-var4 protein was coincided with peroxisomal membrane remnants labeled with EGFP-Pex26p (Fig. 5 F, e–h; Fig. 5 G; Fig. S4 B). Moreover, such membrane remnants were not stained with the markers LC3 and cathepsin D for autophagosomes (Fig. S4 B, a–e) and lysosomes (f–j). These results indicated that the coexpressed HA_2–Miro1-var4 was translocated to the peroxisomal membrane remnants. However, any accumulation of such remnants to the cell periphery was hardly detectable (Fig. 5 F, e–h). Collectively, these results suggest that Pex14p is indispensable for Miro1-var4–mediated peroxisomal movement.

Miro1-var4 interacts with TRAK2, a component of the mitochondrial transport complex

TRAK1 and TRAK2 interact with mitochondrial Miro1-var1 and Miro2 and function as adapters to link mitochondrial Miro proteins and molecular motors, kinesins, and dyneins, thus forming the transport machinery complexes in microtubule-dependent mitochondrial trafficking (Brickley et al., 2005; MacAskill et al., 2009b; Wang and Schwarz, 2009). To investigate whether peroxisome-localized Miro1-var4 interacts with TRAK proteins, HA_2-Miro1 variants were coexpressed with FLAG-tagged TRAK proteins in HEK cells. Immunoprecipitation with anti-FLAG antibody revealed that HA_2–Miro1-var4 interacted with FL-TRAK2 as efficiently as HA_2–Miro1-var1 (Fig. 6 A). FLAG-TRAK2 was mainly localized in tubular network structures, mitochondria in HeLa cells (Fig. 6 B, a and e). Notably, a part of FLAG-TRAK2 was merged with coexpressed

Pex19p binding sites and the core 9-aa residues in typical Pex19p-binding sites in three representative PMPs (Rottensteiner et al., 2004; Halbach et al., 2005) and putative corresponding ones in human Miro1 variants, respectively. The dashed line shows the C terminus of insertion 1. Asterisks and blue letters show highly conserved amino acid residues of putative Pex19p binding sites and leucine^{608}, respectively, in Miro1-var2 and Miro1-var4. An amino acid sequence of the C-terminal region of Miro1-var2 and Miro1-var4 containing a TMD (shaded) and two lysine and arginine residues mutated in KR2S mutants (colored in red) are also shown. **(C)** FL-EGFP-MVC variants and their L608P mutants were synthesized in RRL in the presence of HA_2-Pex19p and immunoprecipitated with anti-FLAG agarose beads as in A. Solid and open arrowheads indicate unmodified and farnesylated HA_2-Pex19p, respectively. **(D)** L608P mutation in insertion 1 impairs peroxisomal localization of Miro1-var2 and Miro1-var4. HeLa cells were transiently transfected with *FLAG-EGFP-MV4C-L608P* (a–d) and *FLAG-EGFP-MV2C-L608P* (e–h) and immunostained using antibodies to Pex14p (b and f, red) and Tom20 (c and g, blue) as in Fig. 1 C. EGFP fluorescence of FL-EGFP-MVCs (a and e, green) and merged views (d and h) are shown. **(E)** In vitro import assay of Miro1 variants was performed by incubating semipermeabilized HeLa cells at 26°C for 1 h with cytosolic fractions each containing FLAG-Pex19p plus HA_2–Miro1-var4 (a and b), HA_2–Miro1-var2 (c and d), or HA_2-Pex26p (e and f). Cells were immunostained with antibodies against HA and Pex14p. Bars, 10 µm. **(F)** Cells shown in E were treated with 0.1 M Na_2CO_3 and separated into soluble (supernatant, S) and membrane (pellet, P) fractions. Equal aliquots of respective fractions were analyzed by immunoblotting with the indicated antibodies.

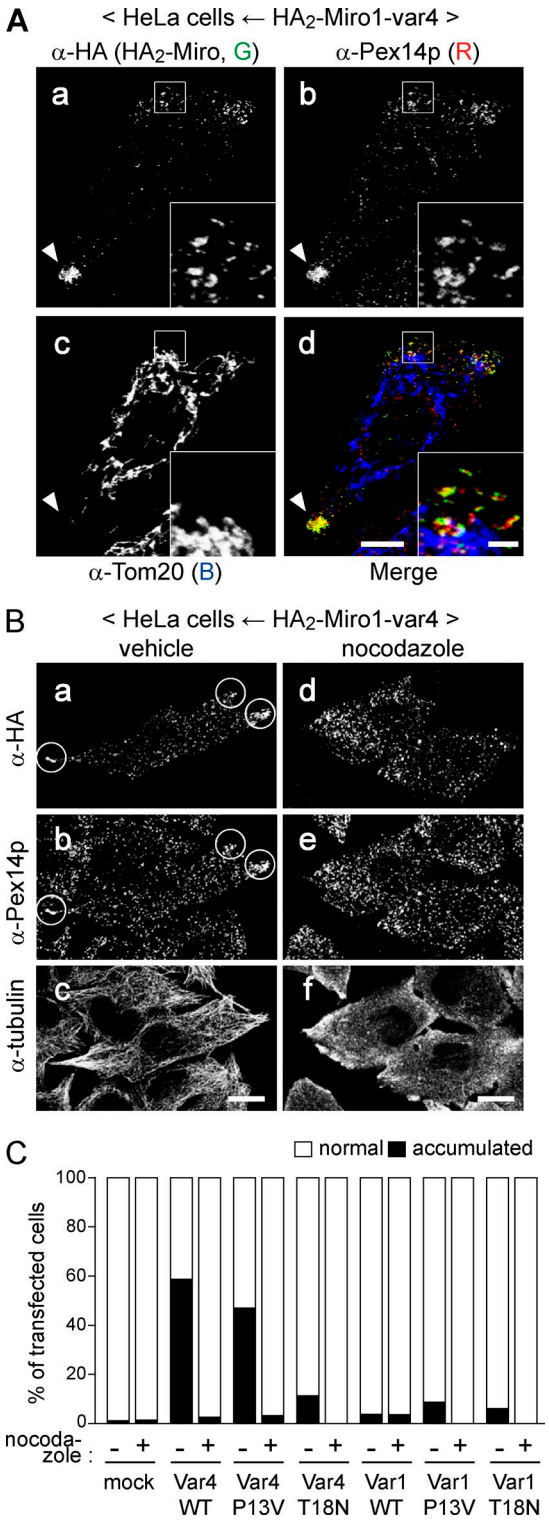

Figure 4. **Miro1-var4 induces accumulation of peroxisomes in the cell periphery. (A)** HeLa cells expressing HA_2–Miro1-var4 were immunostained with antibodies to HA (a, green), Pex14p (b, red), and Tom20 (c, blue) as in Fig. 1 C. The merged image (d) and 3.5-fold magnified views of the boxed areas (insets) were shown. Note that HA_2–Miro1-var4 was often colocalized with Pex14p-positive accumulates of peroxisomes in the cell periphery (arrowheads). **(B)** Nocodazole treatment abrogates Miro1-var4–induced accumulation of peroxisomes at the cell periphery. HeLa cells expressing HA_2–Miro1-var4 as in A were treated with DMSO (vehicle; a–c) or 20 µM nocodazole for 1 h (d–f) and immunostained with antibodies to HA, Pex14p, and α-tubulin. Circles indicate peroxisome-enriched regions in cell periphery. Representative images are shown. Bars: (main images) 10 µm; (insets) 2 µm. **(C)** HeLa cells transfected with an empty vector (mock) or WT and respective GTPase mutants, P13V and T18N of *HA_2–Miro1-var4* and *HA_2–Miro1-var1* were treated with DMSO (–) or nocodazole (+) and immunostained as in B. Percentages of cells exhibiting normal distribution of peroxisomes throughout the cytoplasm (normal, open bar) and accumulation of peroxisomes in the cell periphery (accumulated, solid bar) were represented as the means. Transfected cells ($n \geq 100$) for each condition repeated three times.

HA_2–Miro1-var4 in peroxisomes (Fig. 6 B, arrowheads). To further assess the interaction of endogenous peroxisomal Miro1 variants with TRAK2, HEK cells transiently expressing HA_2-TRAK2 was subjected to immunoprecipitation with anti–Miro1-ins1 antibody. The PNS fraction (Fig. 6 C, lane 2) from the HEK cells was centrifuged at 3,000 *g* to remove the pellet (3K*g* pellet, lane 1), and the resulting supernatant (3K*g* sup, lane 3) was further centrifuged at 100,000 *g* to yield a 100,000-*g* pellet fraction (100K*g* pellet, lane 4). The 100K*g* pellet was enriched in peroxisomes and almost devoid of mitochondria and the cytosol as verified by immunoblotting with antibodies to Pex13p, Tom 20, and LDH (Fig. 6 C, lanes 1–4). The 100k*g* pellet contained endogenous peroxisomal Miro1-var2 (Fig. 6 C, lane 5), and a part of HA_2-TRAK2 associated with light organelles (lanes 1–4). From the 100K*g* pellet fraction, anti–Miro1-ins1 antibody specifically immunoprecipitated endogenous Miro1-var2 together with HA_2-TRAK2 (Fig. 6 C, lanes 6 and 7). Furthermore, the interaction between endogenous Miro1-var2 and HA_2-TRAK2 was also confirmed by immunoprecipitation with anti-HA antibody (Fig. 6 C, lanes 8 and 9). Collectively, these results suggest that peroxisome-localized Miro1-var2 and Miro1-var4 recruit TRAK2 on peroxisomal membrane to form a transport complex involved in peroxisomal movement like that in mitochondrial trafficking.

Discussion

Intracellular transport of peroxisomes is thought to require transport complexes comprising heterogeneous and distinct components such as motor proteins, adapter proteins, and cytoskeleton, depending on the species (Knoblach and Rachubinski, 2015; Neuhaus et al., 2016). In this study, we identified two splicing variants of Miro1 localized to peroxisomes, providing not only the molecular basis for linking peroxisomes and molecular motors for long-distance movement of peroxisomes in mammalian cells but also deeper insight into selective import of TA proteins to peroxisomes and mitochondria.

Depletion of all types of Miro1 variants and reexpression of respective Miro1 variants clearly showed that peroxisomal Miro1 variants are essential components for intracellular transport of peroxisomes (Fig. 5, D and E). Peroxisomal Miro1 variants most likely transport peroxisomes toward the plus ends of the microtubule network in HeLa cells (Figs. 4 and 5), although authentic Miro1-var1 mediates mitochondrial transport in both the anterograde and retrograde directions in mouse hippocampal neurons (Chen and Sheng, 2013). Considering the findings that proper localization of both peroxisomes and mitochondria to neurites is inhibited by elevation of a microtubule-binding protein tau (Stamer et al., 2002) and that Miro1-var4 interacts with TRAK2 as Miro1-var1 does (Fig. 6 A), peroxisomal transport mediated by peroxisomal Miro1 variants most likely

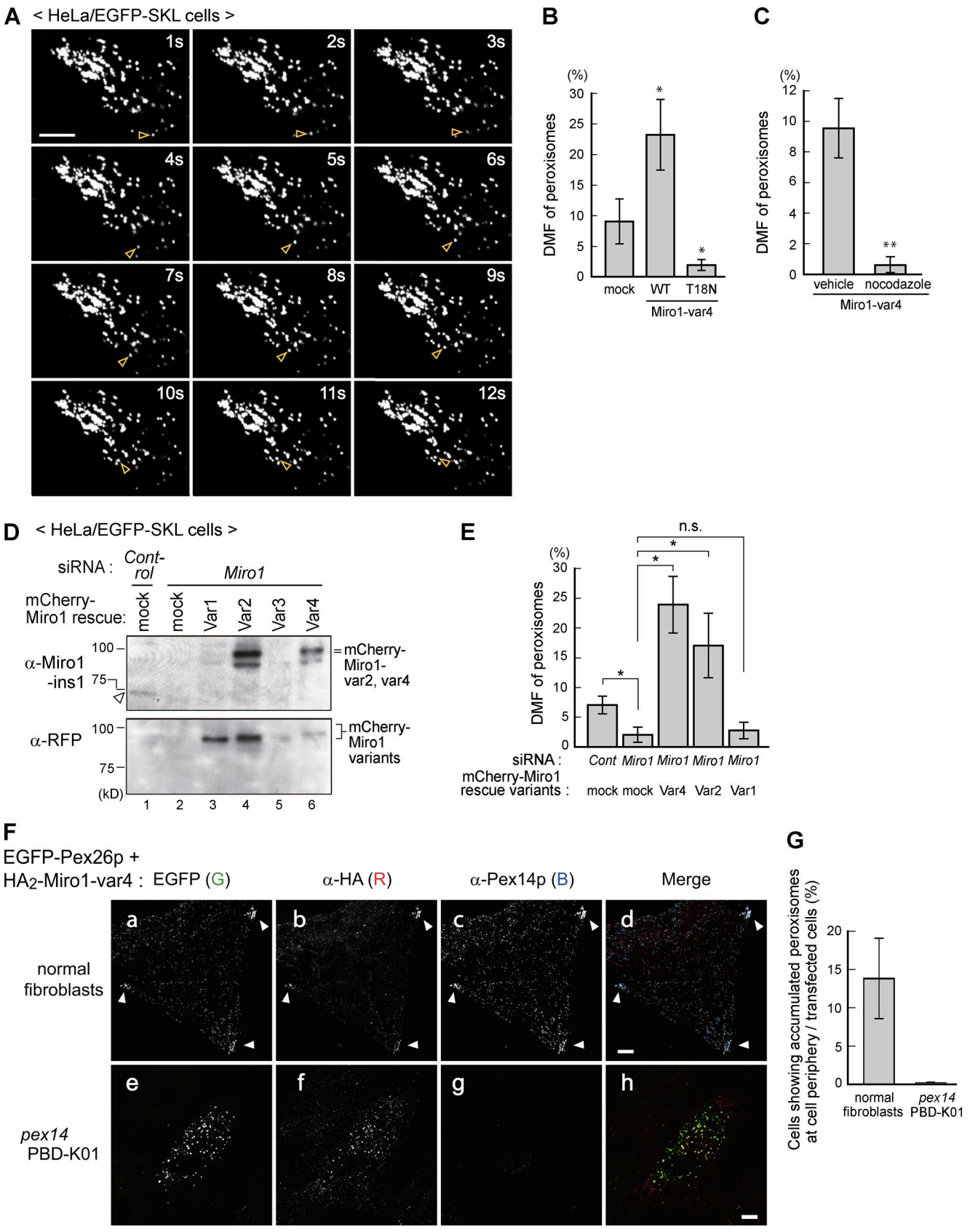

Figure 5. **Miro1-var2 and Miro1-var4 are specifically involved in fast directional movement of peroxisomes in a manner dependent on its GTPase activity and microtubules. (A)** Live imaging of peroxisome movement. Time-lapse images of peroxisomes in HeLa cells stably expressing EGFP-SKL (HeLa/EGFP-SKL) were acquired by confocal fluorescence microscopy at one picture per second. Arrowheads (yellow) indicate a peroxisome showing fast and long-distance movement. Bars, 5 μm. **(B)** HeLa/EGFP-SKL cells were transfected with an empty vector (mock), *mCherry–Miro1-var4–WT* (WT), or *T18N* (T18N) encoding a

shares molecular machineries with mitochondria. However, peroxisomes may be differently regulated in the initiation of organelle movement. In regard to peroxisomal translocation, it is suggested that Pex14p plays a role in anchoring peroxisomes to microtubules (Bharti et al., 2011). Our results suggest that Pex14p indirectly acts upstream of Miro1 variants to evoke peroxisomal movement (Fig. 5 F), although no interaction between Pex14p and the Miro1-var4–TRAK2 complex was observed in vivo (Fig. 6 A). Therefore, it is possible that Pex14p is prerequisite for transition from stationary state to the condition competent to initiate peroxisomal motility, thereby allowing peroxisomal Miro1 variants to form the complexes for peroxisomal transport. In addition, it is noteworthy that most recent studies reporting that the interaction between the peroxisomal TA protein ACBD5 and ER-resident VAMP-associated proteins A and B (VAPA and VAPB) mediates tethering of peroxisomes to the ER and restricts peroxisomal motility (Costello et al., 2017b; Hua et al., 2017). The liberating step of peroxisomes from the ER could be another determinant to initiate peroxisomal movement, where Pex14p and peroxisomal Miro1 variants might be involved.

Mechanisms underlying the regulation with respect to the direction of peroxisomal movement and intracellular positioning remain undefined. Miro1-var1 and Miro2 interacts with the adapter proteins, TRAK1 and TRAK2, both of which mediate kinesin- and dynein-driven transport of mitochondria in both directions (Birsa et al., 2013; Schwarz, 2013; Sheng, 2014). Bidirectional transport of peroxisomes was observed in axon-like processes of mouse human olfactory neural stem cell lines (Wali et al., 2016) and was shown to be regulated by kinesin and dynein motors in *Drosophila melanogaster* S2 cells (Kural et al., 2005; Ally et al., 2009), implying that peroxisomal Miro1 variants are involved in the bidirectional movement of peroxisomes. However, we do not exclude the possibility that any factor or factors other than peroxisomal Miro1 variants participate in peroxisomal transport because peroxisomes distribute, as in control cells, throughout the cytoplasm in *Miro1*-knockout mouse embryonic fibroblasts (Nguyen et al., 2014) and Miro1-depleted HeLa cells (Fig. S4 B). Indeed, dynein-based minus end–directed transport of peroxisomes is suggested in mammalian cells (Schrader et al., 2000; Dietrich et al., 2013). Further studies would be required to delineate precise molecular mechanisms involving such transport.

Insertion 1–dependent targeting of Miro1 splicing variants to peroxisomes extends our knowledge of TA protein import in mammals. Generally, targeting information of TA proteins resides in the TMD and a following luminal tail, where peroxisomal TA requires relatively low hydrophobicity and positive charge in the tail (Yagita et al., 2013, 2017; Chen et al., 2014). We found that the C-terminal region of Miro1-var1 intrinsically targets to mitochondria and that addition of Pex19p binding site–containing insertion 1 consisting of 32 aa in a 53-aa sequence (in Miro1-var4) or 12-aa peptide (in Miro1-var2) upstream of the TMD can alter the destination of Miro1 variants from mitochondria to peroxisomes (Figs. 1 and S2). Importantly, all splicing variants of Miro1 share the same TMD and tail region, indicating that recognition by Pex19p via the cis-acting region is also an important determinant in targeting to the peroxisomal membrane. In regard to peroxisomal targeting of Miro1-var2 and Miro1-var4, the insertion 2 present only in Miro1-var4 enhances peroxisomal import of Miro1-var4, although it is dispensable for mitochondrial localization of Miro1-var3 (Figs. 1 and S2). Despite that Miro1-var4 and Miro1-var2 are similarly recognized by Pex19p in vitro (Fig. 3, A and C), more efficient peroxisomal import of Miro1-var4 appears to be achieved by conformational change of the C-terminal region in combination with the insertion 2. Furthermore, the peroxisomal Miro1 variants appear to be tightly maintained, with their protein level at much lower than mitochondrial Miro1 variants (Fig. 2, A and B). Elevation of Miro1-var4 level readily gives rise to accumulation of peroxisomes in the cell periphery (Fig. 4), which is explained by the finding that a small portion of Miro1-var2 and an undetectable level of Miro1-var4 are present in peroxisomal fractions in HEK cells (Fig. 2, A and B). Such regulation is most likely accomplished by low efficiency of peroxisomal targeting (Figs. 1 and S2) and a minimum level of mRNA expression (Fig. S1 C). Very recently, Costello et al. (2017a) reported that exogenously expressed Myc–Miro1-var1 dually localized to mitochondria and peroxisomes in Cos7 cells. This observation is not consistent with our results. Such contradiction might be a result of the use of different cell lines or the difference of expression levels of Miro1.

Peroxisomes play essential roles in many metabolic functions such as decomposition of a harmful substrate, hydrogen peroxide, and β-oxidation of very long chain fatty acids (Wanders, 2014). Therefore, in analogy to mitochondria, correct transport and intracellular positioning of peroxisomes may be important in polarized cells, especially in neurons. We observed ubiquitous and much fewer levels of mRNA expression of *Miro1-var2* and *Miro1-var4*, respectively, in mouse brains (unpublished data). Interestingly, neuron-specific *Miro1*-knockout mice lacking all splicing variants of Miro1 show that defects in the movement and distribution of mitochondria induce motor neuron disease (Nguyen et al., 2014). In the *Miro1*-deficient neuron of this mouse, mitochondrial distribution is compromised

dominant-negative mutant of the first GTPase domain. At 24 h after transfection, DMF of peroxisomes in mCherry-positive cells was quantified as described in the Live imaging of peroxisomes section of Materials and methods. *, $P < 0.05$ versus mock-treated cells (Student's *t* test). **(C)** HeLa/EGFP-SKL cells expressing WT mCherry–Miro1-var4 were treated for 1 h with DMSO (vehicle) or 20 µM nocodazole as in Fig. 4 B. DMF of peroxisomes was analyzed as in B. **, $P < 0.01$ versus vehicle-treated cells (Student's *t* test). **(D)** Expression of mCherry-Miro1 variants. HeLa/EGFP-SKL cells were treated for 72 h with control siRNA (lane 1) or *Miro1* siRNA against all of the Miro1 variants (lanes 2–6). Cells were then transfected with an empty vector (mock, lanes 1 and 2) or plasmids encoding an siRNA-resistant version of mCherry-Miro1 variants (mCherry-Miro1 rescue variants, lanes 3–6) as indicated at the top. After further 24-h culture, cells were lysed and analyzed by SDS-PAGE and immunoblotting with anti–Miro1-ins1 antibody (top) and anti-RFP antibody (bottom). The arrowhead indicates endogenous Miro1-var2. **(E)** HeLa/EGFP-SKL cells were transfected with *Miro1* siRNA and plasmids encoding mCherry-Miro1 rescue variants as in D. At 24 h after transfection of plasmids, DMF of peroxisomes was analyzed as in B. Data are shown as means ± SD (error bars). Cells ($n \geq 6$) for each condition in three independent experiments. *, $P < 0.05$ (one-way ANOVA followed by a Dunnett's test). **(F)** Accumulation of peroxisomes at the cell periphery requires Pex14p and Miro1-var4. Normal fibroblasts (a–d) and fibroblasts from a *PEX14*-deficient patient (PBD-K01; e–h) were cotransfected with *EGFP-PEX26* and *HA_2–Miro1-var4* for 48 h and immunostained with antibodies to HA (b and f; red) and Pex14p (c and g; blue). EGFP fluorescence of EGFP-Pex26p (a and e; green) and merged views (d and h) are shown. Arrowheads indicate accumulated peroxisomes in the cell periphery (a–d). Representative images are shown. Bars, 10 µm. **(G)** Percentages of cells showing accumulation of peroxisomes in the cell periphery in F are represented as means ± SD (error bars). Cells ($n \geq 20$) for each condition in three independent experiments.

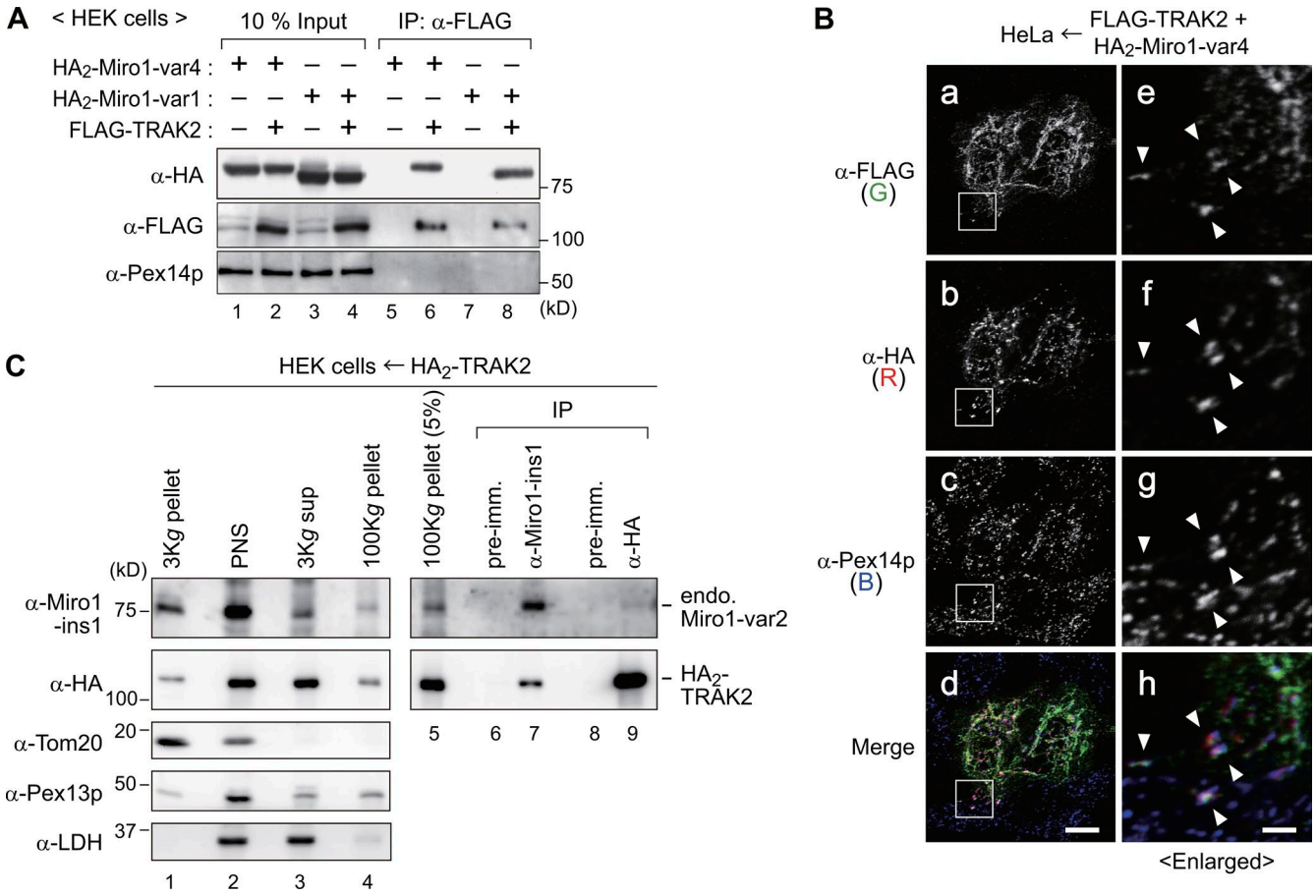

Figure 6. **TRAK2 interacts and colocalizes with Miro1-var4 on peroxisomes. (A)** HEK cells were transfected with *HA_2–Miro1-var4* or *HA_2–Miro1-var1* with or without *FLAG-TRAK2* as indicated at the top. At 24 h after transfection, cells were solubilized and subjected to immunoprecipitation with anti-FLAG antibody. Immunoprecipitates (IPs; lanes 5–8) and the input (10%; lanes 1–4) were analyzed by SDS-PAGE and immunoblotting with antibodies as indicated on the left. **(B)** HeLa cells were cotransfected for 24 h with *HA_2–Miro1-var4* and *FLAG-TRAK2* and immunostained with antibodies to FLAG (a and e; green), HA (b and f; red), and Pex14p (c and g; blue). Merged images were shown (d and h), and the boxed areas were fivefold magnified (e–h). Bars: (a–d) 10 µm; (e–h) 2 µm. Arrowheads indicate colocalization of FLAG-TRAK2 with HA_2–Miro1-var4 in peroxisomes in the cell periphery region. **(C)** A PNS fraction (lane 2) from HEK cells transiently expressing HA_2-TRAK2 was centrifuged at 3,000 *g* and separated into supernatant (3K*g* sup; lane 1) and pellet (3K*g* pellet; lane 3) fractions as in Fig. 2 C. The 3K*g* sup fraction was further centrifuged at 100,000 *g* to yield a cytosol-free pellet fraction (100K*g* pellet; lane 4). The resulting 100K*g* pellet was solubilized and subjected to immunoprecipitation with antisera to Miro1-ins1 (lane 7), HA (lane 9), and their respective preimmune sera (pre-imm.; lanes 6 and 8). Equal-volume aliquots of separated fractions (lanes 1–4) and the immunoprecipitates (lanes 6–9) together with the input of the 100K*g* pellet (5%; lane 5) were analyzed by SDS-PAGE and immunoblotting with antibodies indicated on the left.

because of the defect of retrograde mitochondrial transport (Nguyen et al., 2014). Based on our findings, it is plausible that peroxisomal movement and distribution are also disturbed in Miro1-deficient neurons of *Miro1*-knockout mouse, possibly leading to the pathogenesis of the mouse brain. Deficiency of peroxisome biogenesis causes severe Zellweger spectrum disorders with multiple neurological defects including the impaired neuronal migration in the cerebellum and cerebral cortex (Wanders, 2014; Berger et al., 2016). Moreover, distribution of peroxisomes to the distal region in primary neurons is inhibited by knockout of *PEX13* (Nguyen et al., 2006) and overexpression of tau (Stamer et al., 2002). Similarly, transport of peroxisomes in axonlike processes of human olfactory neural stem cell lines is impaired by a mutation in *SPAST* encoding a microtubule-severing protein, spatin, in hereditary spastic paraplegia (Abrahamsen et al., 2013; Fan et al., 2014). These findings suggest a crucial role of peroxisomal movement and distribution in the progression of neurological dysfunction in peroxisome biogenesis disorders and neurodegenerative diseases.

Materials and methods

Cell culture, DNA transfection, and RNAi

HeLa cells, HEK cells, human skin fibroblasts from a normal control, and a patient with peroxisome biogenesis disorder with *PEX14* deficiency (K-01; Shimozawa et al., 2004) were cultured in DMEM (Invitrogen) supplemented with 10% FBS at 37°C under 5% CO_2 and 95% air. CHO-K1 cells were cultured in Ham's F-12 medium supplemented with 10% FBS. DNA was transfected with Lipofectamine 2000 (Invitrogen) for HeLa and HEK cells and Lipofectamine reagent (Invitrogen) for CHO-K1 cells according to the manufacturer's instructions. DNA transfection into fibroblasts was performed by a NEPA21 type II electroporator (Nepagene) at setting of 150 V and 5 ms using a 2-mm gap cuvette. Knockdown of *Miro1* in HeLa cells was conducted by transfection of Stealth RNAi siRNA (Invitrogen) with Lipofectamine 2000 according to the manufacturer's instructions. The sequence of siRNA for human *Miro1* was 5′-UAACCAAAUCGUCGAAGCACA GUCC-3′. Stealth RNAi Negative Control Medium GC Duplex (Invitrogen) was used as a control.

Plasmids

All plasmids used in this study were constructed by standard methods and verified by DNA sequencing. Primers used for PCR were shown in Table S1. cDNAs encoding human Miro1, its splicing variants, Miro2, TRAK1, and TRAK2 were obtained by RT-PCR using total RNA from HEK cells. Amplified cDNAs each coding for full-length Miro1 splicing variants, Miro1-var2ΔTMD (residues at 2–624 aa), Miro1-var4ΔTMD (residues at 2–665 aa), and full-length Miro2 were cloned into the BamHI–XhoI sites in a pcDNA3.1Zeo$^+$/HA_2-Ub vector (Okumoto et al., 2014) by replacing the ubiquitin-encoding fragment, generating pcDNA3.1Zeo-based plasmids encoding N-terminally HA_2-tagged Miro1 variants and full-length Miro2. cDNA encoding TRAK1 and TRAK2 were likewise cloned into pcDNA3.1Zeo$^+$/FLAG-Ub vector and pcDNA3.1Zeo$^+$/HA_2-Ub vector (Okumoto et al., 2014) at the BamHI–XhoI and BamHI–NotI sites, respectively, generating pcDNA3.1Zeo/FLAG-TRAK1, pcDNA3.1Zeo/FLAG-TRAK2, and pcDNA3.1Zeo/HA_2-TRAK2. cDNAs encoding Miro1 splicing variants were also ligated into the BamHI–XhoI sites in a modified pcDNA3.1Zeo$^+$ vector (Invitrogen) encoding an N-terminal mCherry tag derived from an mCherry-C1 vector (Takara Bio Inc.), generating pcDNA3.1Zeo vector–encoding mCherry-Miro1 variants. The nontagged version of Miro1 variants was generated by cloning cDNAs of full-length Miro1 variants into the BamHI–XhoI sites in a pcDNA3.1Zeo$^+$ vector. HA_2-Miro1 variants each harboring mutations P13V, T18N, L608P, or two KR2S (K648S/R650S in Miro1-var2 and K689S/R691S in Miro1-var4) and siRNA-resistant mutants of mCherry-Miro1 variants in pcDNA3.1Zeo vector were generated by overlapping extension PCR (Ho et al., 1989). To construct FLAG-EGFP–fused C-terminal regions of Miro1 variants, DNA fragments coding for the regions encompassing residues at 574 aa to their respective C terminus were PCR amplified and cloned into the BamHI–XhoI sites of a modified pcDNA3.1Zeo$^+$ vector encoding N-terminal FLAG-EGFP tag. Plasmids pcDNAZeo/FLAG-PEX19 (Yagita et al., 2013), pcDNAZeo/HA_2-PEX19 (Matsuzono et al., 2006), pcDNAZeo/HA_2-PEX26 (Yagita et al., 2013), and EGFP-PEX26 (Yagita et al., 2013) were also used.

Semiquantitative PCR

DNA fragments corresponding with those encoding several C-terminal regions of human Miro1 were amplified by RT-PCR using a pair of primers, quantitative PCR (qPCR)-Miro1-Fw and qPCR-Miro1-Rv (Table S1), and total RNA from HeLa cells as a template. Amplified DNA fragments were separated by electrophoresis in 1% agarose gel, stained with ethidium bromide, and visualized with a FAS-II imaging system (Nippon Genetics).

Antibodies

Rabbit polyclonal antibodies to C-terminal 19-aa residues of Pex14p (Shimizu et al., 1999), Pex13p (Mukai and Fujiki, 2006), Pex3p (Ghaedi et al., 2000), acyl-CoA oxidase (Tsukamoto et al., 1990), HA (Otera et al., 2000), LC3 (MBL), cathepsin D (a gift from K. Kato; Nishimura et al., 1987), and guinea pig anti-Pex14p antibody (Mukai et al., 2002) were used. Rabbit antiserum to the insertion 1 in human Miro1-var2 and Miro1-4, termed anti–Miro1-ins1 antibody, was raised by conventional subcutaneous injection of a synthetic 32-aa peptide (EDHYRDRLSRDMGHTDRIENLRKIWVFLKTAF) that had been linked to keyhole limpet hemocyanin (Tsukamoto et al., 1990). Rabbit antibody was purified by affinity chromatography using a CL-4B column (GE Healthcare) conjugated to GST-Miro1–insertion 1 encompassing the 32-aa sequence according to the manufacturer's instructions. The following primary antibodies were purchased: rabbit polyclonal antibodies to FLAG (Sigma-Aldrich) and Miro1/2 (Santa Cruz Biotechnology, Inc.), mouse monoclonal antibodies to HA (16B12; Covance), FLAG (Sigma-Aldrich), cytochrome P450 reductase (F-10; Santa Cruz Biotechnology, Inc.), α-tubulin (Abcam), and Tom20 (Santa Cruz Biotechnology, Inc.), and goat anti–lactate dehydrogenase antibody (Rockland).

Immunofluorescence microscopy

Immunostaining of cells was performed as described previously (Okumoto et al., 2011) using 4% paraformaldehyde for cell fixation and 0.1% Triton X-100 or 25 µg/ml digitonin for permeabilization. Immune complexes were visualized using Alexa Fluor 488– or 568–labeled goat anti–rabbit or anti–mouse IgG antibody and Alexa Fluor 647–labeled goat anti–guinea pig IgG antibody (Invitrogen). Cells were observed by a confocal laser microscope (LSM510 with Axio Observer.Z1; ZEISS) equipped with a Plan Apochromat 100× 1.4 NA oil immersion objective lens and argon plus dual HeNe lasers at RT. Images were acquired with Zen software (ZEISS) and prepared using Photoshop (CS4; Adobe). In Figs. 4 C and 5 G, accumulation of peroxisomes at the cell periphery was scored by visually counting the cell showing such morphology.

Live imaging of peroxisomes

HeLa cells stably expressing EGFP fused with a peroxisome targeting signal type-1 at its C terminus, termed HeLa/EGFP-SKL cells (Miyata et al., 2012), were seeded in 35-mm glass-bottomed dishes at 24 h before assays. A confocal scanning laser microscope (LSM510 with Axio Observer.Z1) equipped with a Plan Apochromat 100× 1.4 NA oil immersion objective lens and a thermostatic stage was kept at 37°C and 5% CO_2 was used during the course of the live-imaging experiments. Excitation illumination was from an argon ion laser (488 nm). A total of 300 time-lapse images were acquired for 5 min and focused on one cell (one picture per second) and analyzed with MetaMorph software (Molecular Devices). The total number of peroxisomes in a cell in the first frame and the number of peroxisomes showing movement with a velocity >0.5 µm/s and in distance >2 µm were monitored. We defined an index, DMF, to describe population of peroxisomes with fast and long-distance movement as follows: DMF = (number of peroxisomes with directional movement in 5 min)/(total number of peroxisomes).

Subcellular fractionation

Isopycnic ultracentrifugation using iodixanol gradient was performed as described previously (Hosoi et al., 2017), except using HEK cells and a 19–30% linear gradient of iodixanol (OptiPrep; Sigma-Aldrich). In brief, the PNS of HEK cells (~10^7 cells) was prepared with a Potter-Elvehjem homogenizer in buffer H (20 mM Hepes-KOH, pH 7.4, 0.25 M sucrose, 1 mM DTT, and complete protease inhibitor cocktail [Roche]). A 19–30% linear iodixanol gradient was created in a 14 × 89 mm centrifuge tube (Beckman Coulter) by a Gradient Master (Biocomp) according to the manufacturer's protocol. The PNS fraction was suspended in 35% iodixanol solution and was placed beneath the linear gradient and centrifuged at 100,000 *g* for 90 min at 4°C in a SW41Ti rotor (Beckman Coulter). The gradient was collected into 12 fractions. Organelles in each fraction were pelleted down for immunoblot analysis by diluting with an equal volume of buffer H and centrifugation at 100,000 *g* for 20 min at 4°C.

To analyze the topology of peroxisomal Miro1 variants, the PNS fraction of HEK cells was centrifuged at 3,000 *g* for 10 min at 4°C to yield a 3,000-*g* supernatant (3K*g* sup) fraction almost excluding mitochondria. The 3,000-*g* supernatant fraction was treated with 1 M NaCl or 0.1 M Na_2CO_3 for alkaline extraction (Fujiki et al., 1982) on ice for 30 min and separated into soluble and membrane fractions by ultracentrifugation at 100,000 *g* for 30 min at 4°C. A protease protection assay was then performed by incubating the 3,000-*g* supernatant fraction with 100 µg/ml trypsin for 30 min on ice in the absence or presence

of 0.1% Triton X-100. For immunoprecipitation of endogenous Miro1 variants in peroxisomes, the PNS fraction of HEK cells was separated into supernatant (3K*g* sup) and pellet (3K*g* pellet) fractions by centrifugation at 3,000 *g* for 10 min at 4°C as described above. The 3K*g* sup fraction was further centrifuged at 100,000 *g* for 30 min at 4°C to yield a 100,000-*g* pellet (100K*g* pellet) fraction. Separation of cytosolic and organelle fractions from CHO-K1 cells was performed by incubating the harvested cells for 10 min on ice with buffer H containing 100 µg/ml digitonin followed by ultracentrifugation at 100,000 *g* for 30 min at 4°C as described previously (Liu et al., 2016).

Cell-free synthesis of proteins

A quick-coupled transcription/translation system (T_NT T7; Promega) was used for in vitro transcription/translation reactions in RRL according to the manufacturer's instructions. Miro1 variants and Pex26p were synthesized in the reaction mixtures supplemented with RRL-synthesized Pex19p to synthesize proteins in the presence Pex19p at 10% of the final reaction volume as described previously (Yagita et al., 2013). After centrifugation at 100,000 *g* for 30 min at 4°C, the supernatant was used for the immunoprecipitation.

In vitro import assay using semiintact cells

HeLa cells were semipermeabilized as described previously (Matsuzaki and Fujiki, 2008). In brief, cells cultured on 18-mm glass coverslips were incubated for 10 min on ice with 5% BSA in buffer S (0.25 M sucrose, 25 mM Hepes-KOH, pH 7.4, 2.5 mM EGTA, 2.5 mM magnesium acetate, 50 mM KCl, and 1 mM DTT). After washing with ice-cold buffer S, cells were incubated with 50 µg/ml digitonin in buffer S for 5 min at RT, washed three times with ice-cold buffer S, and incubated in buffer S for 30 min on ice. PNS fractions of HeLa cells expressing Pex19p and Miro1 variants were prepared as HEK cells using buffer S, and the cytosolic fractions were isolated by ultracentrifugation at 100,000 *g* for 30 min at 4°C. Semiintact HeLa cells were incubated for 1 h at 26°C with the cytosolic fractions. After extensive wash with buffer S, cells were fixed for immunofluorescence microscopy or subjected to alkaline extraction as described in the Subcellular fractionation section.

Immunoprecipitation

For immunoprecipitation from cell lysates, cells expressing FLAG-tagged Miro1 variants or TRAK2 were lysed in buffer L (40 mM Hepes-KOH, pH 7.4, 0.15 M NaCl, 0.5% Triton X-100, 1 mM EDTA, 1 mM DTT, and the protease inhibitor cocktail [1 mM PMSF and 10 µg/ml each of aprotinin, leupeptin, and pepstatin]). Cell lysates were centrifuged at 20,000 *g* for 10 min at 4°C to remove insoluble cell debris. Resulting supernatants were mixed with anti-FLAG antibody–conjugated agarose beads (Sigma-Aldrich) and incubated at 4°C for 1 h. After washing with buffer L, proteins bound to the beads were eluted with buffer L containing 100 µg/ml FLAG peptide (Sigma-Aldrich) and analyzed by SDS-PAGE and immunoblotting. For immunoprecipitation of endogenous Miro1 variants in peroxisomes, a 100,000-*g* pellet (100K*g* pellet) fraction from PNS fraction of HEK cells transiently expressing HA_2-TRAK2 was lysed in buffer L. After centrifugation at 20,000 *g* for 10 min at 4°C, resulting supernatants were incubated with antibody to Miro1-ins1 or HA in buffer L for 4 h at 4°C. Antibody–antigen complexes were recovered by incubating for 1 h at 4°C with Protein A Sepharose CL-4B (GE Healthcare) and eluted with Laemmli sample buffer. For immunoprecipitation using cell-free synthesized proteins, in vitro translation products were incubated with anti-FLAG antibody–conjugated agarose beads after dilution with buffer C (0.1% CHAPS, 20 mM Hepes-KOH, pH 7.4, 0.15 M KCl, 1 mM EDTA, 1 mM DTT, 10% glycerol, and protease inhibitor cocktail). After washing with buffer C, immunoprecipitates were analyzed by SDS-PAGE and immunoblotting.

Statistical analysis

Quantitative data were represented as means ± SD from at least three independent experiments. Statistical significance was determined using a two-tailed unpaired Student's *t* test or one-way ANOVA with Dunnett's post hoc test. P-values of <0.05 were considered statistically significant.

Online supplemental material

Fig. S1 shows information on DNA and protein sequences of human Miro-1 variants and mRNA level of Miro1 variants in HEK cells. Fig. S2 shows peroxisomal localization of FL-EGFP-MVC variants and membrane topology of Miro1-var4. Fig. S3 shows that both L608P and KR2S mutations inhibit peroxisomal localization of Miro1 variants. Fig. S4 shows localization of mCherry-Miro1 variants in normal cells, localization of Miro1-var4 in *PEX14*-deficient fibroblasts, and morphology of peroxisomes and mitochondria in Miro1-knockdown cells. Video 1 shows peroxisomal movement in control cells. Video 2 shows that Miro1-var4 expression enhances peroxisomal movement. Video 3 shows peroxisomal movement in control siRNA-treated cells. Video 4 shows decreased peroxisomal movement in Miro1-knockdown cells. Videos 5 and 6 show that the lowered peroxisomal movement in Miro1-knockdown cells was restored by expression of Miro1-var4 and Miro1-var2, respectively. Table S1 shows the primers and the sequences used in this study.

Acknowledgments

We thank Dr. K. Kato for rabbit anti–cathepsin D antibody. We also thank S. Okuno for technical assistance, K. Shimizu for preparing figures, and the other members of our laboratory for discussions.

This work was supported in part by grants from the Ministry of Education, Culture, Sports, Science and Technology of Japan, Grants-in-aid for Scientific Research, MEXT KAKENHI Grant Number JP26116007 (to Y. Fujiki) and the Japan Society for the Promotion of Science Grants-in-aid for Scientific Research, Japan Society for the Promotion of Science KAKENHI grants JP24770130, JP26440032, and JP17K07310 (to K. Okumoto) and JP24247038, JP25112518, JP25116717, JP15K14511, JP15K21743, and JP17H03675 (to Y. Fujiki) as well as grants from the Takeda Science Foundation, the Naito Foundation, the Japan Foundation for Applied Enzymology, and the Novartis Foundation (Japan) for the Promotion of Science (to Y. Fujiki).

The authors declare no competing financial interests.

Author contributions: K. Okumoto, T. Ono, A. Shimomura, A. Nagata, and R. Toyama performed experiments. K. Okumoto, T. Ono, A. Shimomura, A. Nagata, R. Toyama, and Y. Fujiki analyzed data. K. Okumoto, T. Ono, and Y. Fujiki conceived the project and wrote the manuscript with contributions from all authors.

Submitted: 21 August 2017
Revised: 27 October 2017
Accepted: 6 November 2017

References

Abrahamsen, G., Y. Fan, N. Matigian, G. Wali, B. Bellette, R. Sutharsan, J. Raju, S.A. Wood, D. Veivers, C.M. Sue, and A. Mackay-Sim. 2013. A patient-derived stem cell model of hereditary spastic paraplegia with *SPAST* mutations. *Dis. Model. Mech.* 6:489–502. https://doi.org/10.1242/dmm.010884

Ally, S., A.G. Larson, K. Barlan, S.E. Rice, and V.I. Gelfand. 2009. Opposite-polarity motors activate one another to trigger cargo transport in live cells. *J. Cell Biol.* 187:1071–1082. https://doi.org/10.1083/jcb.200908075

Babic, M., G.J. Russo, A.J. Wellington, R.M. Sangston, M. Gonzalez, and K.E. Zinsmaier. 2015. Miro's N-terminal GTPase domain is required for

transport of mitochondria into axons and dendrites. *J. Neurosci.* 35:5754–5771. https://doi.org/10.1523/JNEUROSCI.1035-14.2015

Berger, J., F. Dorninger, S. Forss-Petter, and M. Kunze. 2016. Peroxisomes in brain development and function. *Biochim. Biophys. Acta.* 1863:934–955. https://doi.org/10.1016/j.bbamcr.2015.12.005

Bharti, P., W. Schliebs, T. Schievelbusch, A. Neuhaus, C. David, K. Kock, C. Herrmann, H.E. Meyer, S. Wiese, B. Warscheid, et al. 2011. PEX14 is required for microtubule-based peroxisome motility in human cells. *J. Cell Sci.* 124:1759–1768. https://doi.org/10.1242/jcs.079368

Birsa, N., R. Norkett, N. Higgs, G. Lopez-Domenech, and J.T. Kittler. 2013. Mitochondrial trafficking in neurons and the role of the Miro family of GTPase proteins. *Biochem. Soc. Trans.* 41:1525–1531. https://doi.org/10.1042/BST20130234

Borgese, N., and E. Fasana. 2011. Targeting pathways of C-tail-anchored proteins. *Biochim. Biophys. Acta.* 1808:937–946. https://doi.org/10.1016/j.bbamem.2010.07.010

Brambillasca, S., M. Yabal, P. Soffientini, S. Stefanovic, M. Makarow, R.S. Hegde, and N. Borgese. 2005. Transmembrane topogenesis of a tail-anchored protein is modulated by membrane lipid composition. *EMBO J.* 24:2533–2542. https://doi.org/10.1038/sj.emboj.7600730

Brickley, K., M.J. Smith, M. Beck, and F.A. Stephenson. 2005. GRIF-1 and OIP106, members of a novel gene family of coiled-coil domain proteins: association *in vivo* and *in vitro* with kinesin. *J. Biol. Chem.* 280:14723–14732. https://doi.org/10.1074/jbc.M409095200

Chen, Y., and Z.H. Sheng. 2013. Kinesin-1-syntaphilin coupling mediates activity-dependent regulation of axonal mitochondrial transport. *J. Cell Biol.* 202:351–364. https://doi.org/10.1083/jcb.201302040

Chen, Y., L. Pieuchot, R.A. Loh, J. Yang, T.M. Kari, J.Y. Wong, and G. Jedd. 2014. Hydrophobic handoff for direct delivery of peroxisome tail-anchored proteins. *Nat. Commun.* 5:5790. https://doi.org/10.1038/ncomms6790

Costello, J.L., I.G. Castro, F. Camões, T.A. Schrader, D. McNeall, J. Yang, E.-A. Giannopoulou, S. Gomes, V. Pogenberg, N.A. Bonekamp, et al. 2017a. Predicting the targeting of tail-anchored proteins to subcellular compartments in mammalian cells. *J. Cell Sci.* 130:1675–1687. https://doi.org/10.1242/jcs.200204

Costello, J.L., I.G. Castro, C. Hacker, T.A. Schrader, J. Metz, D. Zeuschner, A.S. Azadi, L.F. Godinho, V. Costina, P. Findeisen, A. Manner, M. Islinger, and M. Schrader. 2017b. ACBD5 and VAPB mediate membrane associations between peroxisomes and the ER. *J. Cell Biol.* 216:331-342. https://doi.org/10.1083/jcb.201607055

Dietrich, D., F. Seiler, F. Essmann, and G. Dodt. 2013. Identification of the kinesin KifC3 as a new player for positioning of peroxisomes and other organelles in mammalian cells. *Biochim. Biophys. Acta.* 1833:3013–3024. https://doi.org/10.1016/j.bbamcr.2013.08.002

Fagarasanu, A., M. Fagarasanu, G.A. Eitzen, J.D. Aitchison, and R.A. Rachubinski. 2006. The peroxisomal membrane protein Inp2p is the peroxisome-specific receptor for the myosin V motor Myo2p of *Saccharomyces cerevisiae*. *Dev. Cell.* 10:587–600. https://doi.org/10.1016/j.devcel.2006.04.012

Fagarasanu, A., F.D. Mast, B. Knoblach, Y. Jin, M.J. Brunner, M.R. Logan, J.N. Glover, G.A. Eitzen, J.D. Aitchison, L.S. Weisman, and R.A. Rachubinski. 2009. Myosin-driven peroxisome partitioning in *S. cerevisiae*. *J. Cell Biol.* 186:541–554. https://doi.org/10.1083/jcb.200904050

Fan, Y., G. Wali, R. Sutharsan, B. Bellette, D.I. Crane, C.M. Sue, and A. Mackay-Sim. 2014. Low dose tubulin-binding drugs rescue peroxisome trafficking deficit in patient-derived stem cells in Hereditary Spastic Paraplegia. *Biol. Open.* 3:494–502. https://doi.org/10.1242/bio.20147641

Fransson, A., A. Ruusala, and P. Aspenström. 2003. Atypical Rho GTPases have roles in mitochondrial homeostasis and apoptosis. *J. Biol. Chem.* 278:6495–6502. https://doi.org/10.1074/jbc.M208609200

Fransson, S., A. Ruusala, and P. Aspenström. 2006. The atypical Rho GTPases Miro-1 and Miro-2 have essential roles in mitochondrial trafficking. *Biochem. Biophys. Res. Commun.* 344:500–510. https://doi.org/10.1016/j.bbrc.2006.03.163

Fujiki, Y., A.L. Hubbard, S. Fowler, and P.B. Lazarow. 1982. Isolation of intracellular membranes by means of sodium carbonate treatment: application to endoplasmic reticulum. *J. Cell Biol.* 93:97–102. https://doi.org/10.1083/jcb.93.1.97

Fujiki, Y., K. Okumoto, S. Mukai, M. Honsho, and S. Tamura. 2014. Peroxisome biogenesis in mammalian cells. *Front. Physiol.* 5:307. https://doi.org/10.3389/fphys.2014.00307

Ghaedi, K., S. Tamura, K. Okumoto, Y. Matsuzono, and Y. Fujiki. 2000. The peroxin pex3p initiates membrane assembly in peroxisome biogenesis. *Mol. Biol. Cell.* 11:2085–2102. https://doi.org/10.1091/mbc.11.6.2085

Glater, E.E., L.J. Megeath, R.S. Stowers, and T.L. Schwarz. 2006. Axonal transport of mitochondria requires milton to recruit kinesin heavy chain and is light chain independent. *J. Cell Biol.* 173:545–557. https://doi.org/10.1083/jcb.200601067

Halbach, A., S. Lorenzen, C. Landgraf, R. Volkmer-Engert, R. Erdmann, and H. Rottensteiner. 2005. Function of the PEX19-binding site of human adrenoleukodystrophy protein as targeting motif in man and yeast. PMP targeting is evolutionarily conserved. *J. Biol. Chem.* 280:21176–21182. https://doi.org/10.1074/jbc.M501750200

Halbach, A., C. Landgraf, S. Lorenzen, K. Rosenkranz, R. Volkmer-Engert, R. Erdmann, and H. Rottensteiner. 2006. Targeting of the tail-anchored peroxisomal membrane proteins PEX26 and PEX15 occurs through C-terminal PEX19-binding sites. *J. Cell Sci.* 119:2508–2517. https://doi.org/10.1242/jcs.02979

Hegde, R.S., and R.J. Keenan. 2011. Tail-anchored membrane protein insertion into the endoplasmic reticulum. *Nat. Rev. Mol. Cell Biol.* 12:787–798. https://doi.org/10.1038/nrm3226

Hirokawa, N., Y. Noda, Y. Tanaka, and S. Niwa. 2009. Kinesin superfamily motor proteins and intracellular transport. *Nat. Rev. Mol. Cell Biol.* 10:682–696. https://doi.org/10.1038/nrm2774

Ho, S.N., H.D. Hunt, R.M. Horton, J.K. Pullen, and L.R. Pease. 1989. Site-directed mutagenesis by overlap extension using the polymerase chain reaction. *Gene.* 77:51–59. https://doi.org/10.1016/0378-1119(89)90358-2

Hosoi, K.I., N. Miyata, S. Mukai, S. Furuki, K. Okumoto, E.H. Cheng, and Y. Fujiki. 2017. The VDAC2-BAK axis regulates peroxisomal membrane permeability. *J. Cell Biol.* 216:709–722. https://doi.org/10.1083/jcb.201605002

Hua, R., D. Cheng, É. Coyaud, S. Freeman, E. Di Pietro, Y. Wang, A. Vissa, C.M. Yip, G.D. Fairn, N. Braverman, et al. 2017. VAPs and ACBD5 tether peroxisomes to the ER for peroxisome maintenance and lipid homeostasis. *J. Cell Biol.* 216:367–377. https://doi.org/10.1083/jcb.201608128

Jones, J.M., J.C. Morrell, and S.J. Gould. 2004. PEX19 is a predominantly cytosolic chaperone and import receptor for class 1 peroxisomal membrane proteins. *J. Cell Biol.* 164:57–67. https://doi.org/10.1083/jcb.200304111

Kardon, J.R., and R.D. Vale. 2009. Regulators of the cytoplasmic dynein motor. *Nat. Rev. Mol. Cell Biol.* 10:854–865. https://doi.org/10.1038/nrm2804

Kemper, C., S.J. Habib, G. Engl, P. Heckmeyer, K.S. Dimmer, and D. Rapaport. 2008. Integration of tail-anchored proteins into the mitochondrial outer membrane does not require any known import components. *J. Cell Sci.* 121:1990–1998. https://doi.org/10.1242/jcs.024034

Knoblach, B., and R.A. Rachubinski. 2015. Motors, anchors, and connectors: orchestrators of organelle inheritance. *Annu. Rev. Cell Dev. Biol.* 31:55–81. https://doi.org/10.1146/annurev-cellbio-100814-125553

Kural, C., H. Kim, S. Syed, G. Goshima, V.I. Gelfand, and P.R. Selvin. 2005. Kinesin and dynein move a peroxisome in vivo: a tug-of-war or coordinated movement? *Science.* 308:1469–1472. https://doi.org/10.1126/science.1108408

Liu, Y., Y. Yagita, and Y. Fujiki. 2016. Assembly of peroxisomal membrane proteins via the direct Pex19p-Pex3p pathway. *Traffic.* 17:433–455. https://doi.org/10.1111/tra.12376

MacAskill, A.F., K. Brickley, F.A. Stephenson, and J.T. Kittler. 2009a. GTPase dependent recruitment of Grif-1 by Miro1 regulates mitochondrial trafficking in hippocampal neurons. *Mol. Cell. Neurosci.* 40:301–312. https://doi.org/10.1016/j.mcn.2008.10.016

MacAskill, A.F., J.E. Rinholm, A.E. Twelvetrees, I.L. Arancibia-Carcamo, J. Muir, A. Fransson, P. Aspenstrom, D. Attwell, and J.T. Kittler. 2009b. Miro1 is a calcium sensor for glutamate receptor-dependent localization of mitochondria at synapses. *Neuron.* 61:541–555. https://doi.org/10.1016/j.neuron.2009.01.030

Matsuzaki, T., and Y. Fujiki. 2008. The peroxisomal membrane protein import receptor Pex3p is directly transported to peroxisomes by a novel Pex19p- and Pex16p-dependent pathway. *J. Cell Biol.* 183:1275–1286. https://doi.org/10.1083/jcb.200806062

Matsuzono, Y., T. Matsuzaki, and Y. Fujiki. 2006. Functional domain mapping of peroxin Pex19p: interaction with Pex3p is essential for function and translocation. *J. Cell Sci.* 119:3539–3550. https://doi.org/10.1242/jcs.03100

Miyata, N., K. Okumoto, S. Mukai, M. Noguchi, and Y. Fujiki. 2012. AWP1/ZFAND6 functions in Pex5 export by interacting with cys-monoubiquitinated Pex5 and Pex6 AAA ATPase. *Traffic.* 13:168–183. https://doi.org/10.1111/j.1600-0854.2011.01298.x

Mukai, S., and Y. Fujiki. 2006. Molecular mechanisms of import of peroxisome-targeting signal type 2 (PTS2) proteins by PTS2 receptor Pex7p and PTS1 receptor Pex5pL. *J. Biol. Chem.* 281:37311–37320. https://doi.org/10.1074/jbc.M607178200

Mukai, S., K. Ghaedi, and Y. Fujiki. 2002. Intracellular localization, function, and dysfunction of the peroxisome-targeting signal type 2 receptor,

Pex7p, in mammalian cells. *J. Biol. Chem.* 277:9548–9561. https://doi.org/10.1074/jbc.M108635200

Neuhaus, A., C. Eggeling, R. Erdmann, and W. Schliebs. 2016. Why do peroxisomes associate with the cytoskeleton? *Biochim. Biophys. Acta.* 1863:1019–1026. https://doi.org/10.1016/j.bbamcr.2015.11.022

Nguyen, T., J. Bjorkman, B.C. Paton, and D.I. Crane. 2006. Failure of microtubule-mediated peroxisome division and trafficking in disorders with reduced peroxisome abundance. *J. Cell Sci.* 119:636–645. https://doi.org/10.1242/jcs.02776

Nguyen, T.T., S.S. Oh, D. Weaver, A. Lewandowska, D. Maxfield, M.-H. Schuler, N.K. Smith, J. Macfarlane, G. Saunders, C.A. Palmer, et al. 2014. Loss of Miro1-directed mitochondrial movement results in a novel murine model for neuron disease. *Proc. Natl. Acad. Sci. USA.* 111:E3631–E3640. https://doi.org/10.1073/pnas.1402449111

Nishimura, Y., M. Higaki, and K. Kato. 1987. Identification of a precursor form of cathepsin D in microsomal lumen: characterization of enzymatic activation and proteolytic processing in vitro. *Biochem. Biophys. Res. Commun.* 148:335–343. https://doi.org/10.1016/0006-291X(87)91115-6

Okumoto, K., S. Misono, N. Miyata, Y. Matsumoto, S. Mukai, and Y. Fujiki. 2011. Cysteine ubiquitination of PTS1 receptor Pex5p regulates Pex5p recycling. *Traffic.* 12:1067–1083. https://doi.org/10.1111/j.1600-0854.2011.01217.x

Okumoto, K., H. Noda, and Y. Fujiki. 2014. Distinct modes of ubiquitination of peroxisome-targeting signal type 1 (PTS1) receptor Pex5p regulate PTS1 protein import. *J. Biol. Chem.* 289:14089–14108. https://doi.org/10.1074/jbc.M113.527937

Otera, H., T. Harano, M. Honsho, K. Ghaedi, S. Mukai, A. Tanaka, A. Kawai, N. Shimizu, and Y. Fujiki. 2000. The mammalian peroxin Pex5pL, the longer isoform of the mobile peroxisome targeting signal (PTS) type 1 transporter, translocates the Pex7p.PTS2 protein complex into peroxisomes via its initial docking site, Pex14p. *J. Biol. Chem.* 275:21703–21714. https://doi.org/10.1074/jbc.M000720200

Rao, M., V. Okreglak, U.S. Chio, H. Cho, P. Walter, and S.-O. Shan. 2016. Multiple selection filters ensure accurate tail-anchored membrane protein targeting. *eLife.* 5:e21301. https://doi.org/10.7554/eLife.21301

Rapp, S., R. Saffrich, M. Anton, U. Jäkle, W. Ansorge, K. Gorgas, and W.W. Just. 1996. Microtubule-based peroxisome movement. *J. Cell Sci.* 109:837–849.

Rottensteiner, H., A. Kramer, S. Lorenzen, K. Stein, C. Landgraf, R. Volkmer-Engert, and R. Erdmann. 2004. Peroxisomal membrane proteins contain common Pex19p-binding sites that are an integral part of their targeting signals. *Mol. Biol. Cell.* 15:3406–3417. https://doi.org/10.1091/mbc.E04-03-0188

Sacksteder, K.A., J.M. Jones, S.T. South, X. Li, Y. Liu, and S.J. Gould. 2000. PEX19 binds multiple peroxisomal membrane proteins, is predominantly cytoplasmic, and is required for peroxisome membrane synthesis. *J. Cell Biol.* 148:931–944. https://doi.org/10.1083/jcb.148.5.931

Saotome, M., D. Safiulina, G. Szabadkai, S. Das, A. Fransson, P. Aspenstrom, R. Rizzuto, and G. Hajnóczky. 2008. Bidirectional Ca^{2+}-dependent control of mitochondrial dynamics by the Miro GTPase. *Proc. Natl. Acad. Sci. USA.* 105:20728–20733. https://doi.org/10.1073/pnas.0808953105

Saxton, W.M., and P.J. Hollenbeck. 2012. The axonal transport of mitochondria. *J. Cell Sci.* 125:2095–2104. https://doi.org/10.1242/jcs.053850

Schrader, M., S.J. King, T.A. Stroh, and T.A. Schroer. 2000. Real time imaging reveals a peroxisomal reticulum in living cells. *J. Cell Sci.* 113:3663–3671.

Schwarz, T.L. 2013. Mitochondrial trafficking in neurons. *Cold Spring Harb. Perspect. Biol.* 5:a011304. https://doi.org/10.1101/cshperspect.a011304

Setoguchi, K., H. Otera, and K. Mihara. 2006. Cytosolic factor- and TOM-independent import of C-tail-anchored mitochondrial outer membrane proteins. *EMBO J.* 25:5635–5647. https://doi.org/10.1038/sj.emboj.7601438

Sheng, Z.H. 2014. Mitochondrial trafficking and anchoring in neurons: New insight and implications. *J. Cell Biol.* 204:1087–1098. https://doi.org/10.1083/jcb.201312123

Shimizu, N., R. Itoh, Y. Hirono, H. Otera, K. Ghaedi, K. Tateishi, S. Tamura, K. Okumoto, T. Harano, S. Mukai, and Y. Fujiki. 1999. The peroxin Pex14p. cDNA cloning by functional complementation on a Chinese hamster ovary cell mutant, characterization, and functional analysis. *J. Biol. Chem.* 274:12593–12604. https://doi.org/10.1074/jbc.274.18.12593

Shimozawa, N., T. Tsukamoto, T. Nagase, Y. Takemoto, N. Koyama, Y. Suzuki, M. Komori, T. Osumi, G. Jeannette, R.J.A. Wanders, and N. Kondo. 2004. Identification of a new complementation group of the peroxisome biogenesis disorders and *PEX14* as the mutated gene. *Hum. Mutat.* 23:552–558. https://doi.org/10.1002/humu.20032

Stamer, K., R. Vogel, E. Thies, E. Mandelkow, and E.-M. Mandelkow. 2002. Tau blocks traffic of organelles, neurofilaments, and APP vesicles in neurons and enhances oxidative stress. *J. Cell Biol.* 156:1051–1063. https://doi.org/10.1083/jcb.200108057

Tsukamoto, T., S. Yokota, and Y. Fujiki. 1990. Isolation and characterization of Chinese hamster ovary cell mutants defective in assembly of peroxisomes. *J. Cell Biol.* 110:651–660. https://doi.org/10.1083/jcb.110.3.651

Wali, G., R. Sutharsan, Y. Fan, R. Stewart, J. Tello Velasquez, C.M. Sue, D.I. Crane, and A. Mackay-Sim. 2016. Mechanism of impaired microtubule-dependent peroxisome trafficking and oxidative stress in *SPAST*-mutated cells from patients with Hereditary Spastic Paraplegia. *Sci. Rep.* 6:27004. https://doi.org/10.1038/srep27004

Wanders, R.J.A. 2014. Metabolic functions of peroxisomes in health and disease. *Biochimie.* 98:36–44. https://doi.org/10.1016/j.biochi.2013.08.022

Wang, X., and T.L. Schwarz. 2009. The mechanism of Ca^{2+}-dependent regulation of kinesin-mediated mitochondrial motility. *Cell.* 136:163–174. https://doi.org/10.1016/j.cell.2008.11.046

Wiemer, E.A.C., T. Wenzel, T.J. Deerinck, M.H. Ellisman, and S. Subramani. 1997. Visualization of the peroxisomal compartment in living mammalian cells: dynamic behavior and association with microtubules. *J. Cell Biol.* 136:71–80. https://doi.org/10.1083/jcb.136.1.71

Yagita, Y., T. Hiromasa, and Y. Fujiki. 2013. Tail-anchored PEX26 targets peroxisomes via a PEX19-dependent and TRC40-independent class I pathway. *J. Cell Biol.* 200:651–666. https://doi.org/10.1083/jcb.201211077

Yagita, Y., K. Shinohara, Y. Abe, K. Nakagawa, M. Al-Owain, F.S. Alkuraya, and Y. Fujiki. 2017. Deficiency of a retinal dystrophy protein, acyl-CoA binding domain-containing 5 (ACBD5), impairs peroxisomal β-oxidation of very-long-chain fatty acids. *J. Biol. Chem.* 292:691–705. https://doi.org/10.1074/jbc.M116.760090